

Option pricing under non-Markovian stochastic volatility models: A deep signature approach

Jingtang Ma^{*}Xianglin Wu[†]Wenyuan Li[‡]

August 22, 2025

Abstract

This paper studies the pricing problem in which the underlying asset follows a non-Markovian stochastic volatility model. Classical partial differential equation methods face significant challenges in this context, as the option prices depend not only on the current state, but also on the entire historical path of the process. To overcome these difficulties, we reformulate the asset dynamics as a rough stochastic differential equation and then represent the rough paths via linear or non-linear combinations of time-extended Brownian motion signatures. This representation transforms a rough stochastic differential equation to a classical stochastic differential equation, allowing the application of standard analytical tools. We propose a deep signature approach for both linear and nonlinear representations and rigorously prove the convergence of the algorithm. Numerical examples demonstrate the effectiveness of our approach for both Markovian and non-Markovian volatility models, offering a theoretically grounded and computationally efficient framework for option pricing.

1 Introduction

The pricing problem lies at the heart of mathematical finance, which is equivalent to computing an expectation such as

$$\mathbb{E}[\Phi(X)] = \mathbb{E}[\Phi(X_t : 0 \leq t \leq T)], \quad (1)$$

where Φ is a sufficiently regular payoff function and T denotes maturity. A typical choice of the underlying asset X is the stochastic volatility model as follows

$$dX_t = f(t, X_t)v_t dW_t + g(t, X_t)v_t dB_t, \quad X_0 = x, \quad 0 < t \leq T, \quad (2)$$

^{*}School of Mathematics, Big Data Laboratory on Financial Security and Behavior (Laboratory of Philosophy and Social Sciences, Ministry of Education), Southwestern University of Finance and Economics, Chengdu, 611130, PR China. Email: mjt@swufe.edu.cn

[†]School of Mathematics, Southwestern University of Finance and Economics, Chengdu, 611130, PR China. Email: 1210202Z1003@smail.swufe.edu.cn

[‡]Corresponding author. Department of Statistics and Actuarial Science, The University of Hong Kong, Pokfulam, Hong Kong, PR China. Email: wylsaas@hku.hk.

where (f, g) is a pair of deterministic functions and W and B are independent Brownian motions in a complete filtered probability space $(\Omega, \mathcal{F}_t, P)$. Here, the randomness in (2) only arises from the two independent Brownian motions, implying that the filtration \mathcal{F}_t is generated by \mathcal{F}_t^W and \mathcal{F}_t^B , the filtration induced by W and B , respectively, i.e. $\mathcal{F}_t = \mathcal{F}_t^W \vee \mathcal{F}_t^B$. As for the volatility process $v_t : 0 \leq t \leq T$, we assume that it is \mathcal{F}_t^W -progressive with bounded sample paths throughout this work. This assumption is very general, as it includes nearly all classical stochastic volatility processes in use, as well as the non-Markovian cases, such as rough volatility processes (see Table 1). The formulation of the volatility process v plays an important role in pricing applications. Specifically, classical models, which are typically Markovian, allow the Feynman-Kac theorem to elegantly connect the pricing problem (1) with the corresponding PDEs. However, this framework faces significant challenges when applied to more complex volatility processes that lack the Markovian and semimartingale structure. To overcome these difficulties, we integrate rough path theory with signature transforms to construct a Markovian representation equivalent to (2), thereby enabling the application of classical mathematical finance tools.

Specifically, we reformulate the dynamic (2) to an rough stochastic differential equation (RSDE) with Lyons' lift (see Lyons et al. (2007) and Bank et al. (2025)) as follows

$$dX_t^{\mathbf{I}} = f(t, X_t^{\mathbf{I}})d\mathbf{I}_t + g(t, X_t^{\mathbf{I}})\mathbf{v}_t^{\mathbf{I}}dB_t, \quad X_0^{\mathbf{I}} = x, \quad 0 < t \leq T, \quad (3)$$

where $\mathbf{I}_t = (I_t, \mathbb{I}_t)$ is the rough lift of the fixed realization integrator $I_t := \int_0^t v_s dW_s$ and $\mathbf{v}_t^{\mathbf{I}}$ is defined by \mathbf{I}_t . Then we express the rough paths in (3) as infinite linear or nonlinear combinations of the time-extended Brownian motion's path signature $(\widehat{\mathbb{W}}_t^\infty)_{t \in [0, T]}$. This signature representation allows us to rewrite the RSDE (3) to a classical SDE and degenerate the non-Markovian model to a Markovian model. For practical purposes, we further truncate the infinite signature representation to the finite signature representation and prove the convergence. Lastly, we provide extensive examples to demonstrate the algorithm's effectiveness and develop a deep signature method that is easily extended to general volatility processes.

The non-Markovian stochastic volatility model lies in the field of rough path theory. Lyons (1998) first develops the theoretical foundations for the deterministic rough differential equations (RDEs). Diehl et al. (2017) extend the rough path framework to stochastic partial differential equations (SPDEs) with probabilistic representations. Friz et al. (2021) introduce the RSDEs to provide a unified approach to SDEs and RDEs and prove the existence and uniqueness of its solution. For more recent work, we refer to Friz et al. (2024), Bugini et al. (2024), Bugini et al. (2024), and Li et al. (2024). In financial applications, Bayer et al. (2025) pioneered the use of RPDEs for option pricing by representing rough paths as weakly geometric ones. These paths were then approximated by Lipschitz continuous paths, although the approximation error remains unquantified.

In this paper, we use a signature transform to study the non-Markovian volatility path. It is a convolution transform capturing the path information up to the current time (see Chen (1957)). By its universal linearization property together

with machine learning techniques, the signature transform enables us to extract realistic path features regardless of the complexity of the volatility models (see, e.g., [Kidger et al. \(2019\)](#), [Tong et al. \(2023\)](#) and [Bayer et al. \(2025\)](#)). While these methods are easy to use, they lack mathematical tractability, precluding the use of classical mathematical finance tools. [Cuchiero et al. \(2023\)](#) rigorously exploit the polynomial nature of generic primary processes and derive a tractable option pricing formula. [Abi Jaber et al. \(2024\)](#) and [Abi Jaber and Gérard \(2025\)](#) further provide signature linear representations for specific stochastic volatility processes with analytical coefficients.

Our transformation of the dynamic process (4) into an RSDE is inspired by the state-of-the-art work [Bank et al. \(2025\)](#). However, our approach differs significantly in the treatment of rough paths within the RSDE framework. Specifically, we represent the rough path exactly through an infinite series of signatures, in contrast to their approach, which approximates the rough path as a weakly geometric rough path with Lipschitz continuous approximations. Our method eliminates the need for such approximations, offering a more precise characterization of the rough path dynamics. In addition, the linear signature representation technique was initially introduced in [Abi Jaber and Gérard \(2025\)](#) and [Abi Jaber et al. \(2024\)](#), but the analytical forms are limited to linear path-dependent equations, such as linear Volterra equations, linear delay equations, and Gaussian Volterra processes. Extending this approach to non-linear path-dependent models, such as the rough Heston and rough Bergomi models, remains an open challenge. To address this, we propose two novel approaches: (i) a deep linear signature approach, which employs neural networks to learn the time-dependent coefficients of a linear signature representation, and (ii) a deep nonlinear signature approach, which directly uses the signature as input to a neural network to capture non-linear dynamics. Numerical experiments demonstrate that the deep nonlinear signature approach significantly outperforms the linear method in terms of accuracy. Furthermore, we provide rigorous convergence proofs for both methods.

Our paper contributes to the existing literature by incorporating the signature transform into the RSDE. This transformation converts a non-Markovian system into an equivalent Markovian framework, thereby enabling the application of the classical PDE method for option pricing. Our contributions can be summarized in three aspects:

- This paper extends classical PDE tools, such as the Feynman-Kac theorem, to address option pricing problems in non-Markovian frameworks by leveraging signature transforms within rough path theory. This approach bridges the gap between traditional stochastic calculus and path-dependent settings, enabling the analysis of complex financial models where standard Markovian assumptions fail.
- We present two innovative neural network-based approaches for volatility process approximation: a deep linear signature approach and a deep nonlinear signature approach. Rigorous convergence proofs are provided.
- We quantify the gap between the infinite signature combinations and their associated PDE solutions via the Feynman-Kac theorem (including both linear and nonlinear cases). This demonstrates the reliability of our method.

The rest of the paper is organized as follows. In Section 2, we formulate the problem by first converting the underlying asset price process into an equivalent RSDE, then connecting it to a classical SDE through signature representations of the rough paths involved in the RSDE. In Section 2.2, the convergence analysis for the truncated signature representations and their corresponding PDE solutions is presented. In Section 3, the European option pricing problem under both Markovian and non-Markovian volatility processes are studied. Section 4 concludes.

2 Representing RSDE with finite linear and nonlinear combinations of signatures

Let $(W_t)_{t \in [0, T]}$ and $(B_t)_{t \in [0, T]}$ be two independent standard Brownian motions. Consider an (\mathcal{F}_t^W) -progressive volatility process $(v_t)_{t \in [0, T]}$ with bounded sample paths, and define the associated integral process $I_t := \int_0^t v_s dW_s$, $t \in [0, T]$. We are interested in the following model

$$dX_t = f(t, X_t) dI_t + g(t, X_t) v_t dB_t, \quad X_0 = x, \quad t \in [0, T], \quad (4)$$

where $f, g \in C^{0,3}([0, T] \times \mathbb{R})$ and $x \in \mathbb{R}^+$ is the initial value at $t = 0$. The SDE (4) is very general, as its volatility process v encompasses all (\mathcal{F}_t^W) -progressive and continuous specifications, including the Ornstein-Uhlenbeck (OU) process, the mean-reverting geometric Brownian motion (mGBM), and the recent rough volatility variants (see, e.g., Table 1).

Let $(X_t)_{t \in [0, T]}$ denote the underlying asset price process, and we consider the European option pricing problem as follows

$$\mathbb{E}^{0, x} [\Phi(X_T)] := \mathbb{E} [\Phi(X_T) | X_0 = x], \quad (5)$$

where Φ is a Lipschitz continuous payoff function and T denotes the maturity. In this paper, we focus on applying the classical PDE method to this pricing problem, leveraging its well-established theoretical foundation and practical applicability. Specifically, we employ the Feynman-Kac theorem to establish an equivalence between the option pricing problem (5) and the solution to the PDE associated with (4). However, the potential non-Markovian nature, arising from the pair (v, I) , invalidates the well-posedness of the PDE solution derived via the Feynman-Kac theorem. To establish the Markovian property for the SDE (4), we begin by introducing the Itô rough path lift of the martingale I and its bracket as follows

$$\begin{aligned} \mathbf{I}_t &= (I_t, \mathbb{I}_t) = (I_t, \iint_{0 < t_1 < t_2 < t} dI_{t_1} dI_{t_2}), \\ [\mathbf{I}]_t &= [I]_t = \int_0^t v_s^2 ds, \quad t \in [0, T]. \end{aligned}$$

Moreover, we give the definition of $\mathbf{v}^{\mathbf{I}}$ for almost every $t \in [0, T]$ as follows

$$\left([\mathbf{I}]_t, \frac{d[\mathbf{I}]_t}{dt}, \sqrt{\frac{d[\mathbf{I}]_t}{dt}} \right) := \left(\int_0^t (\mathbf{v}_s^{\mathbf{I}})^2 ds, (\mathbf{v}_t^{\mathbf{I}})^2, |\mathbf{v}_t^{\mathbf{I}}| \right) = \left(\int_0^t v_s^2 ds, v_t^2, |v_t| \right).$$

Replacing the pair (v, I) in the SDE (4) with $(\mathbf{v}^{\mathbf{I}}, \mathbf{I})$ yields the RSDE as follows

$$dX_t^{\mathbf{I}} = f(t, X_t^{\mathbf{I}})d\mathbf{I}_t + g(t, X_t^{\mathbf{I}})\mathbf{v}_t^{\mathbf{I}}dB_t, \quad X_0^{\mathbf{I}} = x, \quad t \in [0, T], \quad (6)$$

where the differential of the rough path \mathbf{I} is defined by the compensated Riemann–Stieltjes integral (see [Hairer and Friz \(2014\)](#) for details) as follows

$$f(t, X_t^{\mathbf{I}})d\mathbf{I}_t := f(t, X_t^{\mathbf{I}})dI_t + \partial_x f(t, X_t^{\mathbf{I}})f(t, X_t^{\mathbf{I}})d\mathbb{I}_t.$$

The solutions $X(\omega)$ and $X^{\mathbf{I}}(\omega)$ to the SDE (4) and the RSDE (6), respectively, have the same distribution a.e. That is, we have

$$\text{Law}(X_t | \mathcal{F}_T^W \vee \mathcal{F}_t^B)(\omega) = \text{Law}(X_t^{\mathbf{I}} | \mathbf{I}_t = (I_t, \mathbb{I}_t)(\omega)), \quad \forall \omega \in \Omega.$$

For a detailed convergence analysis, we refer to Theorem 3.2 in [Bank et al. \(2025\)](#). As a consequence, the option price (5) can be computed via the RSDE (6) as $\mathbb{E}^{0,x} [\Phi(X_T^{\mathbf{I}})]$.

2.1 Framework for linear signature representation

This section reformulate the RSDE (6) into a more tractable form to compute $\mathbb{E}^{0,x} [\Phi(X_T^{\mathbf{I}})]$. To this end, we introduce the path signature framework. Specifically, let

$$\widehat{\mathbb{W}}_t^\infty(\omega) := (\widehat{\mathbb{W}}_t^{(0)}(\omega), \widehat{\mathbb{W}}_t^{(1)}(\omega), \dots, \widehat{\mathbb{W}}_t^{(n)}(\omega), \dots), \quad t \in [0, T]$$

denote the path signature of the time-extended Brownian motion $\widehat{W}_t(\omega) := (t, W_t(\omega))$, $t \in [0, T]$. Moreover, we assume that the pair (v, I) can be equivalently rewritten as an infinite linear combination of $\widehat{\mathbb{W}}^\infty$ with the time-dependent coefficient $\ell_t := (\ell_t^{(0)}, \ell_t^{(1)}, \dots, \ell_t^{(n)}, \dots)$, i.e. $v_t = \langle \ell_t, \widehat{\mathbb{W}}_t^\infty \rangle$ and $I_t = \int_0^t \langle \ell_s, \widehat{\mathbb{W}}_s^\infty \rangle dW_s$ for $t \in [0, T]$ (see [Abi Jaber and Gérard \(2025\)](#) and [Abi Jaber et al. \(2024\)](#) for details). The time-dependent coefficient is a extended tensor algebra defined within the admissible set $\mathcal{A}(\widehat{\mathbb{W}}^\infty)$, which ensures that the infinite series remains well-defined:

$$\mathcal{A}(\widehat{\mathbb{W}}^\infty) := \left\{ \ell_t : \sum_{n=0}^{\infty} |\langle \ell_t^{(n)}, \widehat{\mathbb{W}}_t^{(n)} \rangle| < \infty \text{ for all } t \in [0, T] \text{ a.s.} \right\}.$$

With the above linear signature representations of (v, I) , the RSDE (6) can be rewritten as follows

$$\begin{aligned} dX_t^{\mathbf{I}} &= f(t, X_t^{\mathbf{I}})d\mathbf{I}_t + g(t, X_t^{\mathbf{I}})\mathbf{v}_t^{\mathbf{I}}dB_t \\ &= f(t, X_t^{\mathbf{I}})dI_t + \partial_x f(t, X_t^{\mathbf{I}})f(t, X_t^{\mathbf{I}})d\mathbb{I}_t + g(t, X_t^{\mathbf{I}})\mathbf{v}_t^{\mathbf{I}}dB_t \\ &= \left(f(t, X_t^{\mathbf{I}}) + \partial_x f(t, X_t^{\mathbf{I}})f(t, X_t^{\mathbf{I}}) \int_0^t \langle \ell_s, \widehat{\mathbb{W}}_s^\infty \rangle dW_s \right) d\left(\int_0^t \langle \ell_s, \widehat{\mathbb{W}}_s^\infty \rangle dW_s \right) + g(t, X_t^{\mathbf{I}}) \langle \ell_t, \widehat{\mathbb{W}}_t^\infty \rangle dB_t \\ &= \left\langle f(t, X_t^{\mathbf{I}})\ell_t + \partial_x f(t, X_t^{\mathbf{I}})f(t, X_t^{\mathbf{I}}) \int_0^t \langle \ell_s, \widehat{\mathbb{W}}_s^\infty \rangle dW_s \ell_t, \widehat{\mathbb{W}}_t^\infty \right\rangle dW_t + \left\langle g(t, X_t^{\mathbf{I}})\ell_t, \widehat{\mathbb{W}}_t^\infty \right\rangle dB_t \\ &= \langle \mathbf{q}_t^f, \widehat{\mathbb{W}}_t^\infty \rangle dW_t + \langle \mathbf{q}_t^g, \widehat{\mathbb{W}}_t^\infty \rangle dB_t, \quad t \in [0, T], \end{aligned} \quad (7)$$

where

$$\mathbf{q}_t^f := f(t, X_t^{\mathbf{I}})\ell_t + \partial_x f(t, X_t^{\mathbf{I}})f(t, X_t^{\mathbf{I}}) \int_0^t \langle \ell_s, \widehat{\mathbb{W}}_s^\infty \rangle dW_s \ell_t, \quad (8)$$

and

$$\mathbf{q}_t^g := g(t, X_t^{\mathbf{I}})\ell_t. \quad (9)$$

Notably, we can derive a numerically equivalent time-independent coefficient ℓ for the linear signature representation of specific volatility processes v through Taylor expansion (see [Abi Jaber and Gérard \(2025\)](#)). Building on this result, we present the Proposition 2.1 to reconstruct the RSDE (6) using the time-independent signature representation coefficient ℓ , namely $v_t = \langle \ell, \widehat{\mathbb{W}}_t^\infty \rangle$, $t \in [0, T]$.

Proposition 2.1 (Linear signature representation with time-independent coefficients). *Let $\widehat{W}_t := (t, W_t)$ be a time extended one-dimensional Brownian motion, and $\widehat{\mathbb{W}}^\infty = (\widehat{\mathbb{W}}^{(0)}, \widehat{\mathbb{W}}^{(1)}, \widehat{\mathbb{W}}^{(2)}, \dots)$ be the infinite sequence of its path signature. Suppose a process v_t can be expressed as $v_t = \langle \ell, \widehat{\mathbb{W}}_t^\infty \rangle$, where $\ell = (\ell^{(0)}, \ell^{(1)}, \ell^{(2)}, \dots)$ is a time-independent tensor in the dual space of the signature algebra. Then the Itô integral $I_t = \int_0^t v_s dW_s$ admits a representation:*

$$I_t = \langle \mathbf{p}, \widehat{\mathbb{W}}_t^\infty \rangle,$$

for some other tensor $\mathbf{p} = (\mathbf{p}^{(0)}, \mathbf{p}^{(1)}, \mathbf{p}^{(2)}, \dots)$ and we have $\ell = \mathbf{p}|_2$, where the blue index indicates the projection onto the direction (see, e.g., [Abi Jaber and Gérard \(2025\)](#), Section 2.1).

Furthermore, the RSDE (6) can be represented as follows

$$d\tilde{X}_t^{\mathbf{I}} = \langle \tilde{\mathbf{q}}_t^f, \widehat{\mathbb{W}}_t^\infty \rangle dW_t + \langle \tilde{\mathbf{q}}_t^g, \widehat{\mathbb{W}}_t^\infty \rangle dB_t, \quad t \in [0, T], \quad (10)$$

where

$$\tilde{\mathbf{q}}_t^f := f(t, \tilde{X}_t^{\mathbf{I}})\ell + \partial_x f(t, \tilde{X}_t^{\mathbf{I}})f(t, \tilde{X}_t^{\mathbf{I}})\mathbf{p} \sqcup \ell, \quad (11)$$

and

$$\tilde{\mathbf{q}}_t^g := g(t, \tilde{X}_t^{\mathbf{I}})\ell. \quad (12)$$

Here, \sqcup denotes the shuffle product for tensors (see, e.g., [Abi Jaber and Gérard \(2025\)](#), Section 2.1).

Proof. See Appendix A.1. □

A key observation here is that by conditioning on the Brownian motion W in equation (7) (i.e., given the sample path ω of W), we can disintegrate the randomness arising from W and obtain a Markovian nature in B for the conditional dynamics. In other words, one can view the dynamic $X^{\mathbf{I}}$ as a diffusion driven by the independent Brownian motion B that is conditioning on the full evolution of W . This interpretation enables us to characterize the conditional

expectation $\mathbb{E}^{0,x} [\Phi(X_T^{\mathbf{I}})]$ through the Feynman–Kac theorem. Specifically, applying Itô’s formula to (7) yields the classical PDE as follows

$$\begin{cases} -\partial_t u &= \frac{1}{2} \left(\langle \mathbf{q}_t^f \sqcup \mathbf{q}_t^f, \widehat{\mathbb{W}}_t^\infty \rangle + \langle \mathbf{q}_t^g \sqcup \mathbf{q}_t^g, \widehat{\mathbb{W}}_t^\infty \rangle \right) \partial_{xx}^2 u, \\ u(T, x) &= \Phi(x). \end{cases} \quad (13)$$

From the Feynman–Kac theorem, we know that any bounded solution $u \in C^{1,2}([0, T] \times \mathbb{R})$ to this PDE has the unique representation

$$u(0, x) = \mathbb{E}^{0,x} [\Phi(X_T^{\mathbf{I}})].$$

In the above analysis, we represent the potential non-Markovian pair (v, I) as infinite linear combinations of signatures. However, in practice, it is impossible to choose the exact representation with an infinite sequence. Therefore, we truncate the infinite representation to finite linear combinations of signatures. Specifically, we introduce the projection $\pi_{\leq N}(\cdot)$ for any extended tensor algebra \mathbf{q} as follows

$$\pi_{\leq N}(\mathbf{q}) = (\pi_0(\mathbf{q}), \dots, \pi_N(\mathbf{q})) = (\mathbf{q}^{(0)}, \dots, \mathbf{q}^{(N)}), \quad (14)$$

where $N \in \mathbb{N}$ denotes the truncation order. With the truncated sequence $\langle \pi_{\leq N}(\ell_t), \widehat{\mathbb{W}}_t^N \rangle$, the SDE (7) becomes

$$dX_t^{\mathbf{I},N} = \langle \pi_{\leq N}(\mathbf{q}_t^f), \widehat{\mathbb{W}}_t^N \rangle dW_t + \langle \pi_{\leq N}(\mathbf{q}_t^g), \widehat{\mathbb{W}}_t^N \rangle dB_t, \quad t \in [0, T], \quad (15)$$

where

$$\pi_{\leq N}(\mathbf{q}_t^f) = f(t, X_t^{\mathbf{I},N}) \pi_{\leq N}(\ell_t) + \partial_x f(t, X_t^{\mathbf{I},N}) f(t, X_t^{\mathbf{I},N}) \int_0^t \langle \pi_{\leq N}(\ell_s), \widehat{\mathbb{W}}_s^N \rangle dW_s \pi_{\leq N}(\ell_t)$$

and

$$\pi_{\leq N}(\mathbf{q}_t^g) = g(t, X_t^{\mathbf{I},N}) \pi_{\leq N}(\ell_t).$$

Moreover, the corresponding PDE (13) becomes

$$\begin{cases} -\partial_t u^N = \frac{1}{2} \left(\langle \pi_{\leq N}(\mathbf{q}_t^f) \sqcup \pi_{\leq N}(\mathbf{q}_t^f), \widehat{\mathbb{W}}_t^N \rangle + \langle \pi_{\leq N}(\mathbf{q}_t^g) \sqcup \pi_{\leq N}(\mathbf{q}_t^g), \widehat{\mathbb{W}}_t^N \rangle \right) \partial_{xx}^2 u^N, \\ u^N(T, x) = \Phi(x), \end{cases} \quad (16)$$

and $u^N(0, x) = \mathbb{E}^{0,x} [\Phi(X_T^{\mathbf{I},N})]$. The case of time-independent linear signature representation can be treated similarly using the truncation sequence $\langle \pi_{\leq N}(\ell), \widehat{\mathbb{W}}_t^N \rangle$.

2.2 Convergence analysis for linear signature representation

In this section, we study the gap between the finite and infinite linear signature representations, along with the solutions to the corresponding PDEs. To this end, we first establish the error bound for truncated linear signature combinations in Theorem 2.1, which serves as the foundation for our subsequent analysis.

Theorem 2.1. Let $(v_t)_{t \in [0, T]}$ be a (\mathcal{F}_t^W) -progressive and continuous stochastic process and $\langle \ell_t, \widehat{\mathbb{W}}_t^\infty \rangle$ be the corresponding infinite linear signature representation. We define the finite linear signature representation of $(v_t)_{t \in [0, T]}$ by the first $N \in \mathbb{N}^+$ order components of its infinite linear signature representation. Then there exists a constant $C((\widehat{W}_t)_{t \in [0, T]}) > 0$ depending on the time-extended Brownian motion path $\widehat{W}_t := (t, W_t)$, such that, for $N > \left| 2C((\widehat{W}_t)_{t \in [0, T]}) \right| - 2$, the upper bound of the gap between the finite and infinite linear signatures representations, denoted by G , can be estimated by

$$G_t^{\ell, N} := \left| \langle \ell_t, \widehat{\mathbb{W}}_t^\infty \rangle - \langle \pi_{\leq N}(\ell_t), \widehat{\mathbb{W}}_t^N \rangle \right| \leq O \left(\frac{\left(2C((\widehat{W}_t)_{t \in [0, T]}) \right)^{N+1}}{(N+1)!} \right).$$

Proof. See Appendix A.2. □

With Theorem 2.1, we can easily give the error bounds for the coefficients in (7) and (15), as stated in Proposition 2.2.

Proposition 2.2. Let \widehat{W}_t , $0 \leq t \leq T$ be a time extended one-dimensional Brownian motion and f, g are defined in a closed and bounded compact set. Then the gap between the infinite linear signature combinations with coefficients $(\mathbf{q}^f, \mathbf{q}^g)$ and their finite counterparts with coefficients $(\pi_{\leq N}(\mathbf{q}^f), \pi_{\leq N}(\mathbf{q}^g))$ can be estimated by

$$\begin{aligned} \left| \langle \mathbf{q}_t^f, \widehat{\mathbb{W}}_t^\infty \rangle - \langle \pi_{\leq N}(\mathbf{q}_t^f), \widehat{\mathbb{W}}_t^N \rangle \right| &\leq \sup_{(s, y) \in \Omega} f(s, y) G_t^{\ell, N} + \sup_{(s, y) \in \Omega} f(s, y) \sup_{(s, y) \in \Omega} \partial_y f(s, y) \\ &\left(\int_0^t \left| \langle \ell_s, \widehat{\mathbb{W}}_s^\infty \rangle \right| dW_s G_t^{\ell, N} + \int_0^t G_s^{\ell, N} dW_s \left| \langle \pi_{\leq N}(\ell_t), \widehat{\mathbb{W}}_t^N \rangle \right| \right), \end{aligned}$$

and

$$\left| \langle \mathbf{q}_t^g, \widehat{\mathbb{W}}_t^\infty \rangle - \langle \pi_{\leq N}(\mathbf{q}_t^g), \widehat{\mathbb{W}}_t^N \rangle \right| \leq \sup_{(s, y) \in \Omega} g(s, y) G_t^{\ell, N},$$

where $N \in \mathbb{N}^+$ denotes the truncation order.

Proof. See Appendix A.3. □

Having established the convergence properties of linear signature approximations in the above, we now investigate how these representation gaps propagate to option pricing. Specifically, we quantify how the truncation errors in linear signature representations affect the gap between the solutions of the PDE (13) and its approximation (16), as in Theorem 2.2.

Theorem 2.2. Assume that $\Phi : \mathbb{R} \rightarrow \mathbb{R}$ is Lipschitz continuous with constant \mathcal{L} and the coefficients of SDEs (7) and (15) satisfy the bounds from Proposition 2.2. Define a constant C such that $C \geq C((\widehat{W}_t)_{t \in [0, T]})$ for all $\omega \in \Omega$, then the gap between the solutions $u(0, x)$ and $u^N(0, x)$ to PDE (13) and (16), respectively, can be estimated by

$$|u(0, x) - u^N(0, x)| \leq \left(\sqrt{T^2 + T} + \sqrt{T} \right) \cdot O \left(\frac{C^{N+1}}{(N+1)!} \right).$$

In particular, this gap decays to 0 as $N \rightarrow \infty$.

Proof. See Appendix A.4. □

We have established the convergence analysis for both time-dependent linear signature representations and their corresponding PDE solutions. The time-independent case follows analogously, thus requiring no further elaboration.

2.3 Nonlinear signature representation

It should be noted that the above analysis is based on the restrictive assumption that the volatility process v admits an infinite linear signature representation. To solve the nonlinear path-dependent model, we introduce the deep nonlinear signature algorithm to approximate (v, I) . Specifically, we define $\mathcal{N}_t^v(\widehat{\mathbb{W}}_t^{\leq N}; \phi_v)$, $t \in [0, T]$ as a nonlinear neural network parameterized by ϕ_v , which takes truncated signature inputs to approximate v_t . For simplicity, we suppress the arguments and denote it as $\mathcal{N}_t^{v,N}$ with no ambiguity, then the RSDE (6) can be approximated by

$$d\widehat{X}_t^{\mathbf{I},N} = \widehat{\mathbf{q}}_t^{f,N} dW_t + \widehat{\mathbf{q}}_t^{g,N} dB_t, \quad t \in [0, T], \quad (17)$$

where

$$\widehat{\mathbf{q}}_t^{f,N} := \left(f(t, \widehat{X}_t^{\mathbf{I},N}) + \partial_x f(t, \widehat{X}_t^{\mathbf{I},N}) f(t, \widehat{X}_t^{\mathbf{I},N}) \int_0^t \mathcal{N}_s^{v,N} dW_s \right) \mathcal{N}_t^{v,N}, \quad (18)$$

and

$$\widehat{\mathbf{q}}_t^{g,N} := g(t, \widehat{X}_t^{\mathbf{I},N}) \mathcal{N}_t^{v,N}. \quad (19)$$

The nonlinear case can be analyzed analogously to obtain the truncated classical PDE via the Feynman-Kac theorem, similar to the linear case described above. Subsequently, we follow Bayraktar et al. (2024) to present the error bound for the truncated nonlinear signature representation in Theorem 2.3.

Theorem 2.3. *Let $(v_t)_{t \in [0, T]}$ be a (\mathcal{F}_t^W) -progressive and continuous stochastic process and $\mathcal{N}_t^v(\widehat{\mathbb{W}}_t^N; \phi_v)$ denotes the neural network approximation with inputs $\widehat{\mathbb{W}}_t^N$ and parameter ϕ_v , we define the approximation error as below:*

$$\mathcal{E}_t^{\mathcal{N},v} := \inf_{\phi_v} \mathbb{E} \left| v_t - \mathcal{N}_t^v(\widehat{\mathbb{W}}_t^N; \phi_v) \right|. \quad (20)$$

We then have the following bound of the error:

$$\mathcal{E}_t^{\mathcal{N},v} \leq \epsilon_t^{\mathcal{N},v} + \epsilon_t^{\mathcal{N},v,N}, \quad (21)$$

where $\epsilon_t^{\mathcal{N},v}$ denotes the error introduced from the neural network at time t , and $\epsilon_t^{\mathcal{N},v,N}$ denotes the error from the truncation of the signature at order N .

Proof. See Appendix A.5. □

The error bounds propagate to the coefficients of the SDE (17) and ultimately to the corresponding PDE, following a pattern similar to the time-dependent linear case, as stated below.

Theorem 2.4. Let $\hat{u}^N(0, x) := \mathbb{E}^{0, x} \left[\Phi \left(\hat{X}_T^{\mathbf{I}, N} \right) \right]$, where Φ is a Lipschitz continuous function with constant \mathcal{L} and $\hat{X}^{\mathbf{I}, N}$ satisfies the SDE (17) with N -th order truncated signature inputs. Then the gap between the solutions $u(0, x)$ and $\hat{u}^N(0, x)$ can be estimated by

$$|u(0, x) - \hat{u}^N(0, x)| \leq \left(\sqrt{T^2 + T} + \sqrt{T} \right) \cdot O \left(\sup_{t \in [0, T]} \mathcal{E}_t^{\mathcal{N}, v} \right),$$

where $\mathcal{E}^{\mathcal{N}, v}$ is defined in Theorem 2.3.

Proof. The proof follows directly from the argument presented in Theorem 2.2, requiring no additional elaboration. \square

3 Numerical examples

This section provides illustrative examples of European put option pricing using the linear and nonlinear signature representations of the pair (v, I) . In these examples, we consider various stochastic volatility processes v , which are summarized in Table 1.

Table 1: Examples of the stochastic volatility processes with their corresponding SDEs. Here, v_t is the volatility with initial value $v_0 > 0$, $\alpha = \frac{1}{2} - H \in (0, 1/2)$ and $\kappa, \theta, \sigma, \eta \in \mathbb{R}$.

Model Name	Stochastic Differential Equations
OU (Uhlenbeck and Ornstein, 1930)	$dv_t = \kappa(\theta - v_t)dt + \eta dW_t$
mGBM (Abi Jaber and Gérard, 2025)	$dv_t = \kappa(\theta - v_t)dt + (\eta + \sigma v_t)dW_t$
rHeston (El Euch and Rosenbaum, 2019)	$v_t = v_0 + \int_0^t K(t-s)f(v_s)ds + \int_0^t K(t-s)g(v_s)dW_s,$ $K(t-s) = \frac{(t-s)^{-\alpha}}{\Gamma(1-\alpha)}, \quad f(v_s) = \kappa(\theta - v_s), \quad g(v_s) = \sigma\sqrt{v_s}$
rBergomi (Bayer et al., 2016)	$v_t = v_0 \exp \left(\eta \int_0^t (t-s)^{-\alpha} dW_s \right)$

For discretization, we partition the time interval $[0, T]$ into a uniform grid $\{t_j := j\Delta t, j = 0, 1, \dots, J\}$, where $J \in \mathbb{N}^+$ and $\Delta t = T/J$. And we construct another uniform space-grid $\{x_l := x_0 + l\Delta x, l = 0, 1, \dots, L\}$ on $[x_0, x_L]$

with $x_0, x_L \in \mathbb{R}$ and $x_0 < x_L$, where $L \in \mathbb{N}^+$ and $\Delta x = \frac{x_L - x_0}{L}$. Using the established time-space grid, we give the finite-difference schemes for SDEs and PDEs with linear signature representations in the following subsection.

3.1 Finite-difference schemes for the SDE and PDE with linear signature representations

In this section, we present the discretized SDE (15) and PDE (16) on the time-space grid points (t_j, x_l) , where $j = 0, 1, \dots, J$ and $l = 0, 1, \dots, L$. To simplify notation, we replace the discrete time and space stamps t_j and x_l with their index j and l , respectively.

Now, we can give the discretized SDE (15) as follows

$$X_{j+1}^{\mathbf{I},N} = X_j^{\mathbf{I},N} + \langle \pi_{\leq N}(\ell_j^g), \widehat{\mathbb{W}}_j^N \rangle (B_{j+1} - B_j) + \langle \pi_{\leq N}(\mathbf{q}_j^f), \widehat{\mathbb{W}}_j^N \rangle (W_{j+1} - W_j), \quad (22)$$

where

$$\pi_{\leq N}(\mathbf{q}_j^g) := g(j, X_j^{\mathbf{I},N}) \pi_{\leq N}(\ell_j) \quad (23)$$

and

$$\pi_{\leq N}(\mathbf{q}_j^f) := f(j, X_j^{\mathbf{I},N}) \pi_{\leq N}(\ell_j) + \partial_x f(j, X_j^{\mathbf{I},N}) f(j, X_j^{\mathbf{I},N}) \pi_{\leq N}(\ell_j) \sum_{i=0}^{j-1} \langle \pi_{\leq N}(\ell_i), \widehat{\mathbb{W}}_i^N \rangle (W_{i+1} - W_i). \quad (24)$$

Here, we select $\pi_{\leq N}(\mathbf{q}_j^g)$ and $\pi_{\leq N}(\mathbf{q}_j^f)$ with time-dependent coefficients ℓ_j . The time-independent case involving $\pi_{\leq N}(\tilde{\mathbf{q}}_j^g)$ and $\pi_{\leq N}(\tilde{\mathbf{q}}_j^f)$ can be derived similarly and straightforwardly.

Next, we discretize the PDE (16) by the first-order finite difference scheme with additional Dirichlet boundary conditions. To achieve this, we first define the boundary functions $\psi_0, \psi_L : [0, T] \rightarrow \mathbb{R}$ as follows

$$u(t, x_0) = \psi_0(t), \quad u(t, x_L) = \psi_L(t), \quad u(T, x) = \Phi(x), \quad (t, x) \in [0, T] \times [x_0, x_L].$$

For simplicity, the truncation order argument for u is omitted here. Then we employ the Crank-Nicolson method for discretization, as the explicit scheme was observed to be unstable unless very small time-steps were chosen. Thus, we approximate the spatial derivatives in PDE (16) by central finite difference quotients as follows

$$\delta_x u_j^l := \frac{u_j^{l+1} - u_j^{l-1}}{2\Delta x}, \quad \delta_{xx}^2 u_j^l := \frac{u_j^{l+1} + u_j^{l-1} - 2u_j^l}{(\Delta x)^2} \quad (25)$$

for $j = 0, 1, \dots, J$ and $l = 1, 2, \dots, L-1$. From all things above, the Crank-Nicolson discretization reads

$$\begin{aligned} -\frac{u_{j+1}^l - u_j^l}{\Delta t} &= \frac{1}{4} \left[\left(\langle \pi_{\leq N}(\mathbf{q}_j^f) \sqcup \pi_{\leq N}(\mathbf{q}_j^f), \widehat{\mathbb{W}}_j^N \rangle + \langle \pi_{\leq N}(\mathbf{q}_j^g) \sqcup \pi_{\leq N}(\mathbf{q}_j^g), \widehat{\mathbb{W}}_j^N \rangle \right) \delta_{xx}^2 u_j^l \right. \\ &\quad \left. + \left(\langle \pi_{\leq N}(\mathbf{q}_{j+1}^f) \sqcup \pi_{\leq N}(\mathbf{q}_{j+1}^f), \widehat{\mathbb{W}}_{j+1}^N \rangle + \langle \pi_{\leq N}(\mathbf{q}_{j+1}^g) \sqcup \pi_{\leq N}(\mathbf{q}_{j+1}^g), \widehat{\mathbb{W}}_{j+1}^N \rangle \right) \delta_{xx}^2 u_{j+1}^l \right] \end{aligned} \quad (26)$$

for $0 \leq j \leq J-1, 1 \leq l \leq L-1$, with boundary conditions

$$u_j^0 = \psi_0(t_j), \quad u_j^L = \psi_L(t_j), \quad u_j^l = \Phi(x_l).$$

Following the above discretization framework, we now present the first example with the Markovian volatility processes: OU and mGBM, from Table 1.

EXAMPLE 3.1 (Markovian volatility processes with linear signature representations). *In this example, we first analytically reconstruct the Markovian volatility processes v_t and its integrated counterpart $I_t := \int_0^t v_s dW_s$ using linear signature representations with time-independent coefficients ℓ and \mathbf{p} , respectively. We then incorporate them into the above discretization framework to compute European put option prices. Specifically, we estimate prices by simulating paths via the discretized SDE (22) to evaluate the conditional expectation $\mathbb{E}^{0,x} [\Phi(X_T^I)]$, while the solution to PDE (26) provides equivalent pricing results under the Feynman-Kac theorem.*

For implementation details, we consider the case where the asset-price dynamics (4) follow the SABR dynamics, i.e., $f(t, x) = \rho x^\beta$ and $g(t, x) = \sqrt{1 - \rho^2} x^\beta$ for some $\beta \in (\frac{1}{2}, 1)$. And the volatility process v follows either the OU or mGBM process as specified in Table 1. We set the time and space step size as $\Delta t = 1/251$ and $\Delta x = 1/400$, respectively. The parameters for the SABR stochastic volatility model and European put options are specified as follows

$$\kappa = 1, \theta = 0.25, \sigma = 0.01, \eta = 1.2, v_0 = 0.1, \rho = -0.4, \beta = 0.6, K = 110, T = 1,$$

where K is the strike.

We begin by computing the time-independent coefficients ℓ and \mathbf{p} of the linear signature representations \tilde{v} and \tilde{I} . We first consider the case where v follows the OU process, then its linear signature representation \tilde{v} has coefficients of the following algebraic form

$$\tilde{v}_t = \langle \ell^{OU}, \widehat{\mathbb{W}}_t^\infty \rangle, \quad \ell^{OU} = (v_0 \Phi + \kappa \theta \mathbf{1} + \eta \mathbf{2}) e^{\mathbb{L} - \kappa \mathbf{1}}.$$

To be more explicit, the linear form of ℓ^{OU} reads

$$\begin{aligned} \ell^{OU} &= (v_0 \Phi + \kappa \theta \mathbf{1} + \eta \mathbf{2}) \sum_{n=0}^{\infty} \frac{(-\kappa \cdot \mathbf{1})^{\mathbb{L} \mathbb{L} n}}{n!} \\ &= (v_0 \Phi + \kappa \theta \mathbf{1} + \eta \mathbf{2}) (\Phi - \kappa \mathbf{1} + \kappa^2 \mathbf{11} - \kappa^3 \mathbf{111} + \kappa^4 \mathbf{1111} - \kappa^5 \mathbf{11111} + \dots) \\ &= v_0 \cdot \Phi - \kappa(v_0 - \theta) \cdot \mathbf{1} + \eta \cdot \mathbf{2} + \kappa^2(v_0 - \theta) \cdot \mathbf{11} - \kappa \eta \cdot \mathbf{21} \\ &\quad - \kappa^3(v_0 - \theta) \cdot \mathbf{111} + \kappa^2 \eta \cdot \mathbf{211} + \kappa^4(v_0 - \theta) \cdot \mathbf{1111} - \kappa^3 \eta \cdot \mathbf{2111} \\ &\quad - \kappa^5(v_0 - \theta) \cdot \mathbf{11111} + \kappa^4 \eta \cdot \mathbf{21111} + \dots \\ &= \left(v_0, \begin{pmatrix} -\kappa(v_0 - \theta) \\ \eta \end{pmatrix}, \begin{pmatrix} \kappa^2(v_0 - \theta) & 0 \\ -\kappa \eta & 0 \end{pmatrix}, \begin{pmatrix} -\kappa^3(v_0 - \theta) & 0 \\ 0 & 0 \\ \kappa^2 \eta & 0 \\ 0 & 0 \end{pmatrix}, \dots \right), \end{aligned}$$

where the blue letters denote the tensor product of the canonical basis, i.e., $\mathbf{1} \cdots \mathbf{d} := e_1 \otimes \cdots \otimes e_d$ for $d = 1, 2, \dots$

With Proposition 2.1, we can further give the coefficient \mathbf{p}^{OU} of the linear representation \tilde{I} as follows

$$\begin{aligned} \mathbf{p}^{OU} = & v_0 \cdot \mathbf{2} - \kappa(v_0 - \theta) \cdot \mathbf{12} + \eta \cdot \mathbf{22} + \kappa^2(v_0 - \theta) \cdot \mathbf{112} - \kappa\eta \cdot \mathbf{212} \\ & - \kappa^3(v_0 - \theta) \cdot \mathbf{1112} + \kappa^2\eta \cdot \mathbf{2112} + \kappa^4(v_0 - \theta) \cdot \mathbf{11112} - \kappa^3\eta \cdot \mathbf{21112} + \cdots \end{aligned}$$

Similarly, the mGBM process also admits an infinite linear signature representation with coefficients of the following algebraic form

$$\tilde{v}_t = \langle \ell^{mGBM}, \widehat{\mathbb{W}}_t^\infty \rangle, \ell^{mGBM} = \left(v_0 \Phi + \left(\kappa\theta - \frac{\sigma\eta}{2} \right) \mathbf{1} + \eta \mathbf{2} \right) e^{\sqcup \sqcup \left(- \left(\kappa + \frac{\sigma^2}{2} \right) \mathbf{1} + \sigma \mathbf{2} \right)}.$$

The linear form of ℓ^{mGBM} reads

$$\begin{aligned} \ell^{mGBM} &= (v_0 \Phi + \gamma \mathbf{1} + \eta \mathbf{2}) \sum_{n=0}^{\infty} \frac{(\lambda \mathbf{1} + \sigma \mathbf{2})^{\sqcup \sqcup n}}{n!} \\ &= (v_0 \Phi + \gamma \mathbf{1} + \eta \mathbf{2}) \left[\Phi + \lambda \mathbf{1} + \sigma \mathbf{2} + \lambda^2 \mathbf{11} + \lambda \sigma (\mathbf{12} + \mathbf{21}) + \sigma^2 \mathbf{22} \right. \\ &\quad \left. + \lambda^3 \mathbf{111} + \lambda^2 \sigma (\mathbf{112} + \mathbf{121} + \mathbf{211}) + \lambda \sigma^2 (\mathbf{122} + \mathbf{212} + \mathbf{221}) + \sigma^3 \mathbf{222} + \cdots \right] \\ &= v_0 \Phi + (v_0 \lambda + \gamma) \mathbf{1} + (v_0 \sigma + \eta) \mathbf{2} \\ &\quad + \lambda(v_0 \lambda + \gamma) \mathbf{11} + \sigma(v_0 \lambda + \gamma) \mathbf{12} + \lambda(v_0 \sigma + \eta) \mathbf{21} + \sigma(v_0 \sigma + \eta) \mathbf{22} \\ &\quad + \lambda^2(v_0 \lambda + \gamma) \mathbf{111} + \lambda \sigma(v_0 \lambda + \gamma) (\mathbf{112} + \mathbf{121}) + \sigma^2(v_0 \lambda + \gamma) \mathbf{122} \\ &\quad + \lambda^2(v_0 \sigma + \eta) \mathbf{211} + \lambda \sigma(v_0 \sigma + \eta) (\mathbf{212} + \mathbf{221}) + \sigma^2(v_0 \sigma + \eta) \mathbf{222} + \cdots \\ &= \left(v_0, \begin{pmatrix} v_0 \lambda + \gamma \\ v_0 \sigma + \eta \end{pmatrix}, \begin{pmatrix} \lambda(v_0 \lambda + \gamma) & \sigma(v_0 \lambda + \gamma) \\ \lambda(v_0 \sigma + \eta) & \sigma(v_0 \sigma + \eta) \end{pmatrix}, \right. \\ &\quad \left. \begin{pmatrix} \lambda^2(v_0 \lambda + \gamma) & \lambda \sigma(v_0 \lambda + \gamma) \\ \lambda \sigma(v_0 \lambda + \gamma) & \sigma^2(v_0 \lambda + \gamma) \\ & \lambda^2(v_0 \sigma + \eta) & \lambda \sigma(v_0 \sigma + \eta) \\ & \lambda \sigma(v_0 \sigma + \eta) & \sigma^2(v_0 \sigma + \eta) \end{pmatrix}, \cdots \right), \end{aligned}$$

where $\lambda = - \left(\kappa + \frac{\sigma^2}{2} \right)$ and $\gamma = \kappa\theta - \frac{\sigma\eta}{2}$. And we can further derive the coefficient \mathbf{p}^{mGBM} as follows

$$\begin{aligned} \mathbf{p}^{mGBM} = & v_0 \cdot \mathbf{2} + (v_0 \lambda + \gamma) \cdot \mathbf{12} + (v_0 \sigma + \eta) \cdot \mathbf{22} \\ & + \lambda(v_0 \lambda + \gamma) \cdot \mathbf{112} + \sigma(v_0 \lambda + \gamma) \cdot \mathbf{122} + \lambda(v_0 \sigma + \eta) \cdot \mathbf{212} + \sigma(v_0 \sigma + \eta) \cdot \mathbf{222} \\ & + \lambda^2(v_0 \lambda + \gamma) \cdot \mathbf{1112} + \lambda \sigma(v_0 \lambda + \gamma) \cdot \mathbf{1122} \\ & + \lambda \sigma(v_0 \lambda + \gamma) \cdot \mathbf{1212} + \sigma^2(v_0 \lambda + \gamma) \cdot \mathbf{1222} + \cdots \end{aligned}$$

Now, having these explicit coefficients in hand, we can analytically reconstruct v and I with linear signature representations \tilde{v} and \tilde{I} , respectively. We employ a Monte Carlo method with the path number $M = 10000$ and the number of time intervals $J = 251$ as our benchmark and evaluate the path-wise mean absolute error (MAE) ϵ and the overall MAE \mathcal{E} as follows

$$\epsilon(A_{m,\cdot}, \tilde{A}_{m,\cdot}) := \frac{1}{J+1} \sum_{j=0}^J |A_{m,j} - \tilde{A}_{m,j}|, \quad m = 1, \dots, M, \quad (27)$$

$$\mathcal{E}(A, \tilde{A}) := \frac{1}{M} \sum_{m=1}^M \epsilon(A_{m,\cdot}, \tilde{A}_{m,\cdot}), \quad (28)$$

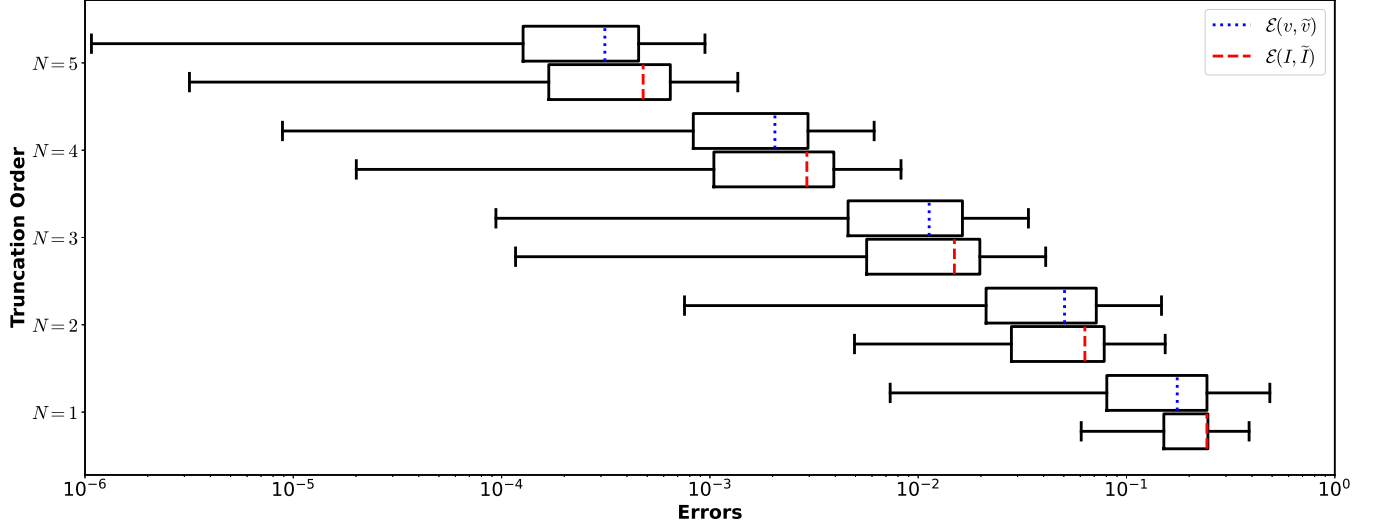
where A and \tilde{A} represent arbitrary matrices containing M paths, each of length $J + 1$. In Figure 1, we plot the distribution of path-wise MAEs ϵ and present the overall MAEs \mathcal{E} between the Monte Carlo sample paths (v, I) and their linear signature representations (\tilde{v}, \tilde{I}) at different truncation levels for both OU and mGBM processes. The corresponding values are detailed in Table 2. The results show that: (1) the accuracy and robustness of linear signature representations \tilde{v} and \tilde{I} (for both OU and mGBM) increases significantly as the truncation level increases; (2) both the \tilde{v} and \tilde{I} of the OU process outperform mGBM's in accuracy at higher truncation levels. These indicate that the accuracy of linear signature representations is sensitive to both the signature truncation level and the type of volatility process.

As outlined previously, we now approximate the European put option prices using (\tilde{v}, \tilde{I}) by substituting them into both the discrete SDE (22) and the PDE (26). That is, we employ SDE (22) for Monte Carlo simulation to compute the conditional expectation $\mathbb{E}^{0,x} [\Phi(X_T^{\mathbf{I},N})]$, while utilizing the solution to PDE (26) as the option price through the Feynman-Kac theorem. As before, we use Monte Carlo-simulated option prices $\mathbb{E}^{0,x} [\Phi(X_T)]$ as the benchmark, measuring approximation accuracy through the absolute error

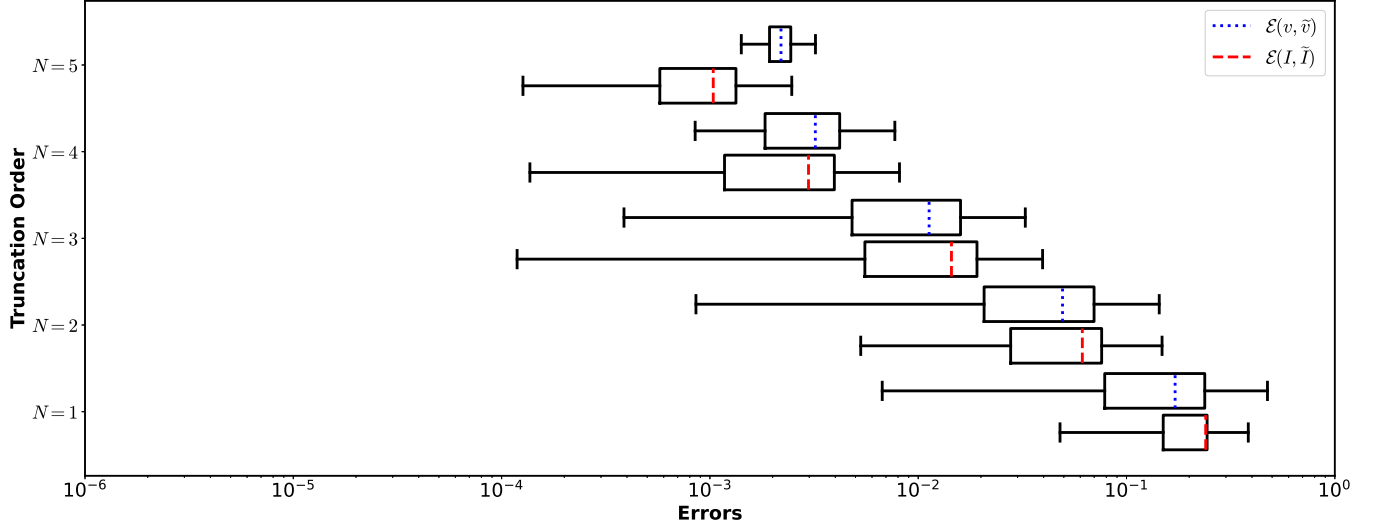
$$\left| \mathbb{E}^{0,x} [\Phi(X_T)] - \mathbb{E}^{0,x} [\Phi(X_T^{\mathbf{I},N})] \right|.$$

Figure 2 shows the approximation errors in option pricing for out-of-the-money (OTM), at-the-money (ATM), and in-the-money (ITM) cases under both the OU process and mGBM across different truncation levels. Detailed results are presented in Table 3.

These reveal four key observations: (1) Both numerical schemes show monotonically decreasing errors with higher truncation levels; (2) The approximations obtained from SDE show competitive accuracy regardless of moneyness, while the accuracy of approximations obtained from PDE show progressively lower accuracy moving from ITM to ATM to OTM; (3) The PDE method outperforms the SDE method in accuracy at lower truncation levels, thus it can provide sufficient accuracy while reducing computational costs by using lower-order signatures in practice; (4) Table 2 shows that the mGBM model has slightly lower accuracy than the OU process in approximating sample paths (v, I) . However, Table 3 reveals that this difference shrinks when evaluating option pricing errors, both models achieve comparable accuracy for European put options.



(a) OU



(b) mGBM

Figure 1: Accuracy of linear signature representations (\tilde{v}, \tilde{I}) for truncation levels $N = 1$ to 5 under (Top:) the OU process and (Bottom:) mGBM: Each box spans from the first quartile (25%) to the third quartile (75%) of path-wise MAEs ϵ . The whisker boundaries denote the maximum and minimum ϵ . The overall MAEs \mathcal{E} are marked out by the dashed (or dotted) lines. The horizontal axis uses a logarithmic scale, and the results are based on the Monte Carlo method with path number $M = 10000$ and the number of time intervals $J = 251$.

Table 2: Overall MAEs \mathcal{E} between (v, I) and (\tilde{v}, \tilde{I}) corresponding to Figure 1 for different truncation levels and volatility processes. Standard deviations of path-wise MAEs ϵ appear in parentheses.

Truncation Level	Errors for OU process		Errors for mGBM	
	$\mathcal{E}(v, \tilde{v})$	$\mathcal{E}(I, \tilde{I})$	$\mathcal{E}(v, \tilde{v})$	$\mathcal{E}(I, \tilde{I})$
$N = 1$	1.75e-1 (1.21e-1)	2.43e-1 (2.02e-1)	1.71e-1 (1.18e-1)	2.40e-1 (1.95e-1)
$N = 2$	5.04e-2 (3.65e-2)	6.31e-2 (5.54e-2)	4.93e-2 (3.57e-2)	6.14e-2 (5.35e-2)
$N = 3$	1.13e-2 (8.29e-3)	1.49e-2 (1.37e-2)	1.13e-2 (8.01e-3)	1.44e-2 (1.32e-2)
$N = 4$	2.05e-3 (1.52e-3)	2.92e-3 (2.69e-3)	3.21e-3 (1.66e-3)	2.97e-3 (2.63e-3)
$N = 5$	3.13e-4 (2.33e-4)	4.78e-4 (4.40e-4)	2.19e-3 (3.64e-4)	1.04e-3 (6.41e-4)

Table 3: The approximation errors corresponding to Figure 2 for different truncation levels and volatility processes.

Model	Truncation Level	Errors obtained from SDE (22)			Errors obtained from PDE (26)		
		ITM	ATM	OTM	ITM	ATM	OTM
OU	$N = 1$	4.62e-1	1.06e+0	1.02e+0	6.89e-1	8.48e-1	4.36e-1
	$N = 2$	1.03e-1	1.76e-1	2.26e-1	1.43e-1	6.69e-2	1.22e-1
	$N = 3$	1.12e-1	8.46e-2	6.46e-2	2.46e-1	1.25e-1	4.56e-2
	$N = 4$	9.66e-2	7.00e-2	7.71e-2	2.24e-1	9.36e-2	5.31e-2
	$N = 5$	9.63e-2	7.56e-2	6.69e-2	2.27e-1	9.76e-2	5.19e-2
mGBM	$N = 1$	9.07e-1	1.10e+0	1.03e+0	7.00e-1	8.78e-1	4.67e-1
	$N = 2$	1.39e-1	1.71e-1	1.93e-1	1.88e-1	6.16e-2	8.17e-2
	$N = 3$	8.81e-2	7.67e-2	5.83e-2	2.85e-1	1.68e-1	3.46e-2
	$N = 4$	7.43e-2	8.04e-2	5.31e-2	2.65e-1	1.37e-1	2.75e-2
	$N = 5$	7.51e-2	9.35e-2	4.61e-2	2.68e-1	1.42e-1	2.76e-2

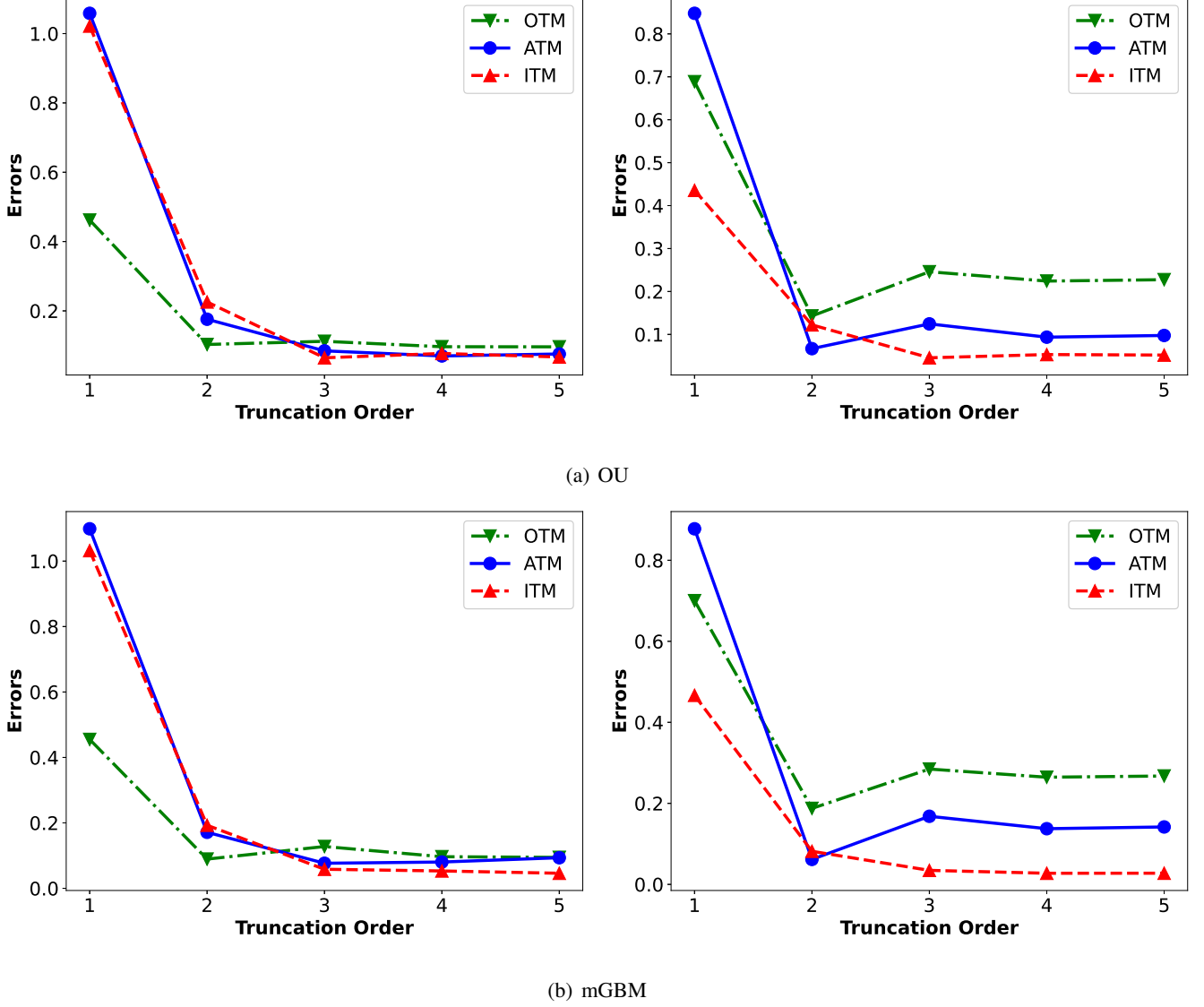


Figure 2: Accuracy of approximations obtained from (Left:) SDE (22) and (Right:) PDE (26) for option prices at different moneyness levels. The analysis considers three cases: ATM ($x = 110 = K$), ITM ($x = 95 < K$), and OTM ($x = 115 > K$).

3.2 Deep learning schemes for linear and nonlinear signature representations

As discussed in Section 2, we employ a neural network \mathcal{N}^v as the nonlinear signature approximation of non-Markovian volatility processes. Specifically, for each time step j , we define the map $\mathcal{N}^v \left(\widehat{\mathbb{W}}_j^N; \phi_v \right) \mapsto \widehat{v}_j^{\text{nonlinear}}$ to directly learn v_j , and its training problem reads

$$\min_{\phi_v} \frac{1}{J} \sum_{j=0}^J \left[\mathcal{N}^v \left(\widehat{\mathbb{W}}_j^N; \phi_v \right) - v_j \right]^2, \quad (29)$$

where ϕ_v is the parameter of $\mathcal{N}^{v,N}$ waiting for training. We present the detailed architecture of $\mathcal{N}^{v,N}$ as follows

- a convolutional layer with 128 channels and kernel size 5;
- a two-layer stacked LSTM with 128 hidden units per layer;
- a fully connected feedforward neural network with 3 hidden layers, each of size 32 and ReLU activation.

We further give the discrete truncated SDE and its associated PDE as follows

$$\widehat{X}_{j+1}^{\mathbf{I},N} = \widehat{X}_j^{\mathbf{I},N} + \widehat{\mathbf{q}}_j^{f,N} (W_{j+1} - W_j) + \widehat{\mathbf{q}}_j^{g,N} (B_{j+1} - B_j), \quad (30)$$

and

$$-\frac{u_{j+1}^l - u_j^l}{\Delta t} = \frac{1}{4} \left[\left((\widehat{\mathbf{q}}_j^{f,N})^2 + (\widehat{\mathbf{q}}_j^{g,N})^2 \right) \delta_{xx}^2 u_j^l + \left((\widehat{\mathbf{q}}_{j+1}^{f,N})^2 + (\widehat{\mathbf{q}}_{j+1}^{g,N})^2 \right) \delta_{xx}^2 u_{j+1}^l \right], \quad (31)$$

where the coefficients reads

$$\widehat{\mathbf{q}}_j^{f,N} := \left[f(j, \widehat{X}_j^{\mathbf{I},N}) + \partial_x f(j, \widehat{X}_j^{\mathbf{I},N}) f(j, \widehat{X}_j^{\mathbf{I},N}) \sum_{i=0}^{j-1} \mathcal{N}_i^{v,N} (W_{i+1} - W_i) \right] \mathcal{N}_j^{v,N}$$

and

$$\widehat{\mathbf{q}}_j^{g,N} := g(j, \widehat{X}_j^{\mathbf{I},N}) \mathcal{N}_j^{v,N}.$$

For comparison, we also introduce the linear signature representations for these non-Markovian volatility processes. Since the coefficients of linear signature representations for complex volatility processes are implicit, we introduce another neural network \mathcal{N}^ℓ with parameters ϕ_ℓ . It shares the same architecture as \mathcal{N}^v but takes different inputs and outputs. Specifically, for each time step j , we have $\mathcal{N}^\ell : (t_j, \widehat{\mathbb{W}}_j^N; \phi_\ell) \mapsto \pi_{\leq N}(\widehat{\ell}_j)$ to learn the coefficients $\pi_{\leq N}(\ell_j)$ for $\lim_{N \rightarrow \infty} \langle \pi_{\leq N}(\ell_j), \widehat{\mathbb{W}}_j^N \rangle = v_j$. And the training problem can be defined as follows

$$\min_{\phi_\ell} \frac{1}{J} \sum_{j=0}^J \left[\langle \mathcal{N}^\ell(t_j, \widehat{\mathbb{W}}_j^N; \phi_\ell), \widehat{\mathbb{W}}_j^N \rangle - v_j \right]^2. \quad (32)$$

In the following example, we will employ these two neural networks to deal with option pricing problems under non-Markovian volatility processes.

EXAMPLE 3.2 (Non-Markovian volatility processes with nonlinear and linear signature representations). *In this example, we first use the previously introduced neural network \mathcal{N}^v and \mathcal{N}^ℓ to represent the non-Markovian pair (v, I) , which denote the nonlinear and linear signature representations, respectively. We then incorporate these signature representations into the corresponding SDE and PDE to compute European put option prices as in Example 3.1.*

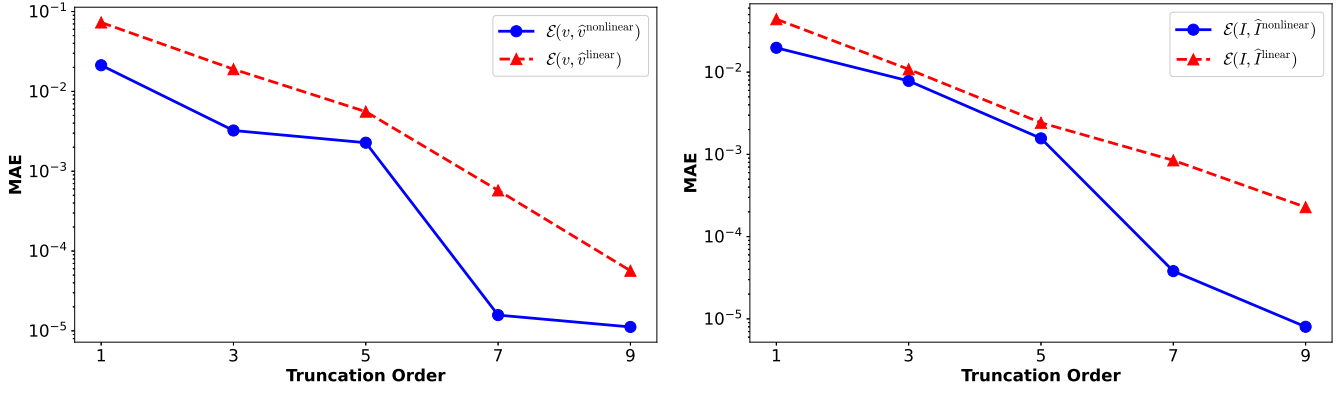
For implementation details, we consider the Riemann-Liouville rHeston volatility process v , as well as the rBergomi process, from Table 1. We set the constants as follows

$$\kappa = 0.1, \theta = 0.25, \sigma = 0.01, \eta = 1, v_0 = 0.1, \alpha = 0.2, \rho = -0.4, \beta = 1, K = 110, T = 1.$$

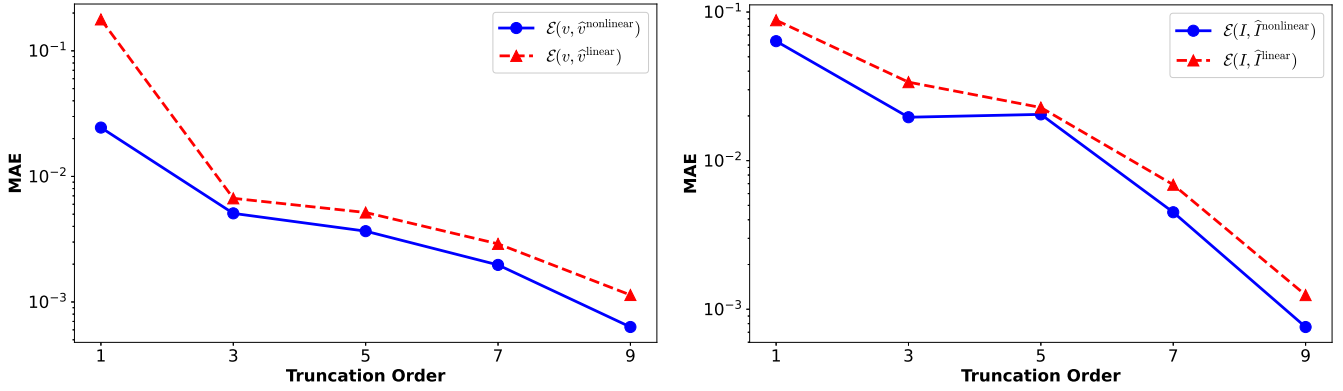
Moreover, we keep the other settings consistent with Example 3.1.

Let $\hat{v}^{\text{nonlinear}}$ and \hat{v}^{linear} denote the nonlinear and linear signature representations, respectively. Then we present the MAE \mathcal{E} between the Monte Carlo benchmark (v, I) and its truncated signature representations at different truncation levels for both rHeston and rBergomi processes in Figure 3. The results show that: (1) the nonlinear signature representation consistently outperforms its linear counterpart in accuracy across all truncation levels for both volatility processes; (2) the accuracy of both the nonlinear and linear signature representations increases significantly as the truncation level increases; (3) the accuracy of both the nonlinear and linear signature representations for the rHeston volatility process is significantly better than that for the rBergomi volatility process. However, as we will show next, this difference shrinks when evaluating option pricing errors, as illustrated in Example 3.1.

Similar to Example 3.1, we incorporate both the nonlinear and linear signature representations into the SDE and PDE for European put options pricing. Moreover, we use $\mathbb{E}^{0,x} \left[\Phi \left(\hat{X}_T^{\mathbf{I}, \text{nonlinear}} \right) \right]$ and $\mathbb{E}^{0,x} \left[\Phi \left(\hat{X}_T^{\mathbf{I}, \text{linear}} \right) \right]$ to denote the option prices obtained from the nonlinear and linear signature representations, respectively. The results are shown in Figure 4 for the rHeston and rBergomi volatility processes, respectively. We observe that the approximation error converges quickly and that a small truncation level, such as $N = 3$, is sufficient for practical purposes. The reason is that both the nonlinear and linear signature representations of the pair (v, I) have achieved sufficiently high accuracy at high truncation orders. Consequently, when these representations are incorporated into the SDE and PDE for option pricing, the errors remain comparable.

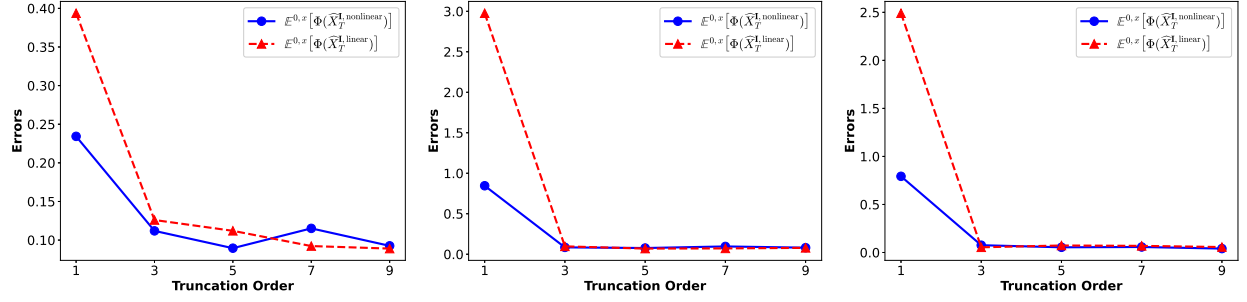


(a) rHeston

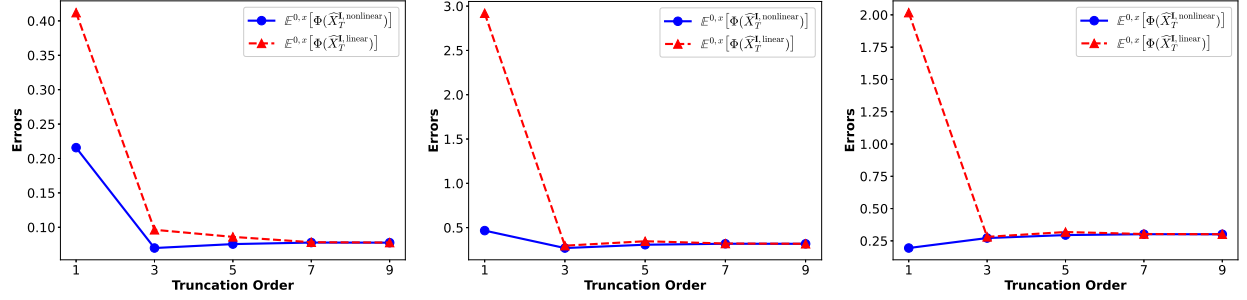


(b) rBergomi

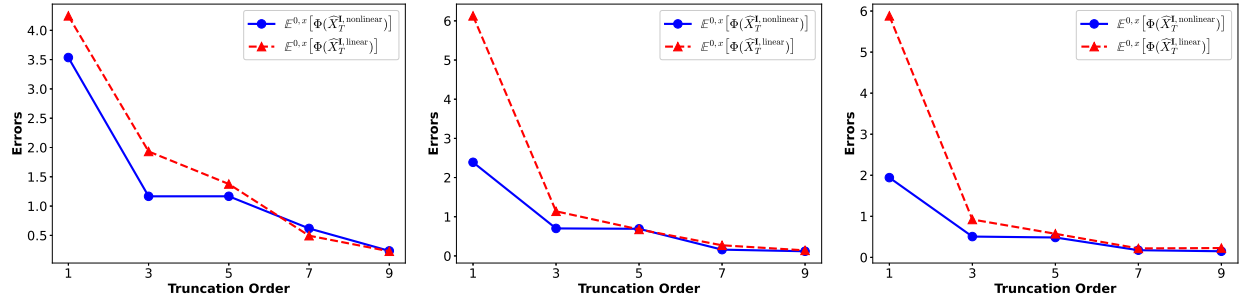
Figure 3: Accuracy of nonlinear signature representations ($\hat{v}^{\text{nonlinear}}, \hat{I}^{\text{nonlinear}}$) and linear signature representations ($\hat{v}^{\text{linear}}, \hat{I}^{\text{nonlinear}}$) for truncation levels $N = 1$ to 9 under (Top:) the rHeston and (Bottom:) rBergomi process. The vertical axis uses a logarithmic scale and the results are based on $M = 10000$ samples.



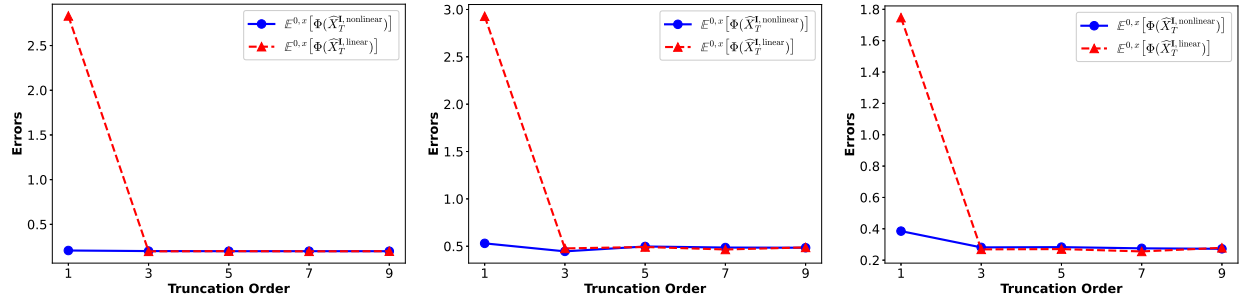
(a) SDE under rHeston



(b) PDE under rHeston



(c) SDE under rBergomi



(d) PDE under rBergomi

Figure 4: Approximation error obtained from SDE and PDE for European put option prices under rHeston and rBergomi volatility processes at different moneyness levels. The analysis considers three cases: (Left:) OTM ($x = 115 > K$), (Middle:) ATM ($x = 110 = K$) and (Right:) ITM ($x = 95 < K$).

4 Conclusions

This paper proposes a deep signature method to solve the European option pricing problem within the framework of general non-Markovian stochastic volatility models. To address the non-Markovian nature of the volatility process, we first reformulate the SDE to an RSDE through Lyons' lift. Using the signature representation, we then transform the RSDE into a classical SDE. Next, we can derive the corresponding PDE with the classical Feynman-Kac theorem for option pricing and employ the finite difference methods to compute the European option prices. For linear Markovian models, such as OU and mGBM, we can obtain the explicit forms of the signature representations. For nonlinear path-dependent models, such as rHeston and rBergomi, we propose two approaches, deep linear signature and deep nonlinear signature methods, to study the non-Markovian volatility. Numerical experiments demonstrate that both methods converge rapidly with increasing signature truncation level, with the deep nonlinear signature method achieving superior accuracy. Furthermore, we provide a comprehensive convergence analysis that incorporates truncation errors of the signature, approximation errors of the signature representation, and the overall pricing error, thereby ensuring the robustness of our framework. Due to the powerful learning capacity of neural networks, our deep signature method is adaptable to more complex scenarios and opens avenues for future research in option pricing under non-Markovian stochastic volatility models.

Acknowledgements

Jingtang Ma acknowledges financial support from the National Natural Science Foundation of China (Grant No. 12071373). Wenyan Li gratefully acknowledges a start-up grant from the University of Hong Kong.

References

- Abi Jaber, E., and Gérard, L. A. (2025). Signature volatility models: pricing and hedging with Fourier. *SIAM Journal on Financial Mathematics*, 16(2), 606-642.
- Abi Jaber, E., Gérard, L. A., and Huang, Y. (2024). Path-dependent processes from signatures. *arXiv preprint arXiv:2407.04956*.
- Bank, P., Bayer, C., Friz, P. K., and Pelizzari, L. (2025). Rough PDEs for local stochastic volatility models. *Mathematical Finance*, 35(3), 661-681.
- Bayer, C., Friz, P., and Gatheral, J. (2016). Pricing under rough volatility. *Quantitative Finance*, 16(6), 887-904.

- Bayer, C., Pelizzari, L., and Zhu, J. J. (2025). Pricing American options under rough volatility using deep-signatures and signature-kernels. *arXiv preprint arXiv:2501.06758*.
- Bayraktar, E., Feng, Q., and Zhang, Z. (2024). Deep signature algorithm for multidimensional path-dependent options. *SIAM Journal on Financial Mathematics*, 15(1), 194-214.
- Bugini, F., Coghi, M., and Nilssen, T. (2024). Malliavin calculus for rough stochastic differential equations. *arXiv preprint arXiv:2402.12056*.
- Bugini, F., Friz, P. K., and Stannat, W. (2024). Parameter dependent rough SDEs with applications to rough PDEs. *arXiv preprint arXiv:2409.11330*.
- Chen, K. T. (1957). Integration of paths, geometric invariants and a generalized Baker-Hausdorff formula. *Annals of Mathematics*, 65(1), 163-178.
- Cuchiero, C., Gazzani, G., and Svaluto-Ferro, S. (2023). Signature-based models: theory and calibration. *SIAM Journal on Financial Mathematics*, 14(3), 910-957.
- Diehl, J., Friz, P. K., and Stannat, W. (2017). Stochastic partial differential equations: a rough paths view on weak solutions via Feynman–Kac. *Annales de la Faculté des Sciences de Toulouse Mathématiques*, 26(4), 911-947.
- El Euch, O., and Rosenbaum, M. (2019). The characteristic function of rough Heston models. *Mathematical Finance*, 29(1), 3-38.
- Friz, P. K., Hocquet, A., and Lê, K. (2021). Rough stochastic differential equations. *arXiv preprint arXiv:2106.10340*.
- Friz, P. K., Lê, K., and Zhang, H. (2024). Controlled rough SDEs, pathwise stochastic control and dynamic programming principles. *arXiv preprint arXiv:2412.05698*.
- Funahashi, K. I., and Nakamura, Y. (1993). Approximation of dynamical systems by continuous time recurrent neural networks. *Neural Networks*, 6(6), 801-806.
- Gatheral, J., Jaisson, T., and Rosenbaum, M. (2018). Volatility is rough. *Quantitative Finance*, 18(6), 933–949.
- Goudenège, L., Molent, A., and Zanette, A. (2022). Moving average options: Machine learning and Gauss-Hermite quadrature for a double non-Markovian problem. *European Journal of Operational Research*, 303(2), 958-974.
- Hairer, M., and Friz, P. (2014). *A Course on Rough Paths with an Introduction to Regularity Structures*. Springer, Berlin.

- Kidger, P., Bonnier, P., Perez Arribas, I., Salvi, C., and Lyons, T. (2019). Deep signature transforms. *Proceedings of the 33rd Neural Information Processing Systems International Conference*, 3105-3115.
- Li, H., Zhang, H., and Zhang, K. (2024). Reflected backward stochastic differential equations with rough drivers. *arXiv preprint arXiv:2407.17898*.
- Lyons, T. J. (1998). Differential equations driven by rough signals. *Revista Matemática Iberoamericana*, 14(2), 215–310.
- Lyons, T. J., Caruana, M., and Lévy, T. (2007). *Differential Equations Driven by Rough Paths*. Springer Berlin Heidelberg.
- Tong, A., Nguyen-Tang, T., Lee, D., Tran, T. M., and Choi, J. (2023). Sigformer: Signature transformers for deep hedging. *Proceedings of the Fourth ACM International Conference on AI in Finance*, 124-132.
- Uhlenbeck, G. E., and Ornstein, L. S. (1930). On the theory of the Brownian motion. *Physical Review*, 36(5), 823-841.
- Yang, W., Ma, J., and Cui, Z. (2025). A general valuation framework for rough stochastic local volatility models and applications. *European Journal of Operational Research*, 322(1), 307-324.

A Appendix

A.1 Proof of Proposition 2.1

Proof. Given $v_t = \langle \ell, \widehat{\mathbb{W}}_t^\infty \rangle = \sum_{n=0}^{\infty} \langle \ell^{(n)}, \widehat{\mathbb{W}}_t^{(n)} \rangle$, we can expand the Itô integral as follows

$$\int_0^t v_s dW_s = \sum_{n=0}^{\infty} \int_0^t \langle \ell^{(n)}, \widehat{\mathbb{W}}_s^{(n)} \rangle dW_s.$$

Recall the definition of n -th order signatures,

$$\widehat{\mathbb{W}}_t^{(n)} = \int_{0 < t_1 < \dots < t_n < t} d\widehat{W}_{t_1} \otimes \dots \otimes d\widehat{W}_{t_n},$$

then we can give the recursive structure of signatures as follows

$$d\widehat{\mathbb{W}}_t^{(n+1)} = \widehat{\mathbb{W}}_t^{(n)} \otimes d\widehat{W}_t.$$

Then the integration against dW_s (the second component of $d\widehat{W}_t = (dt, dW_t)$) corresponds to

$$\int_0^t \langle \ell^{(n)}, \widehat{\mathbb{W}}_s^{(n)} \rangle dW_s = \langle \ell^{(n)}, \int_0^t \widehat{\mathbb{W}}_s^{(n)} dW_s \rangle = \langle \ell^{(n)}, \widehat{\mathbb{W}}_t^{(n+1)} |_{\mathbf{2}} \rangle = \langle \ell^{(n)} \otimes e_2, \widehat{\mathbb{W}}_t^{(n+1)} \rangle,$$

where $e_2 = \begin{pmatrix} 0 \\ 1 \end{pmatrix}$ selects the dW_t component.

Now we define \mathbf{p} by shifting indices as follows

$$\mathbf{p}^{(0)} = 0, \quad \mathbf{p}^{(n+1)} = \boldsymbol{\ell}^{(n)} \otimes e_2, \quad n \geq 0.$$

This yields

$$\int_0^t v_s dW_s = \sum_{n=0}^{\infty} \langle \mathbf{p}^{(n+1)}, \widehat{\mathbb{W}}_t^{(n+1)} \rangle = \langle \mathbf{p}, \widehat{\mathbb{W}}_t^{\infty} \rangle,$$

where $\mathbf{p} = (0, \boldsymbol{\ell}^{(0)} \otimes e_2, \boldsymbol{\ell}^{(1)} \otimes e_2, \dots)$ provides the required representation.

With the linear signature representations of the pair (v, I) , the RSDE (6) can be rewritten as follows

$$\begin{aligned} d\tilde{X}_t^{\mathbf{I}} &= f(t, \tilde{X}_t^{\mathbf{I}}) d\mathbf{I}_t + g(t, \tilde{X}_t^{\mathbf{I}}) \mathbf{v}_t^{\mathbf{I}} dB_t \\ &= f(t, \tilde{X}_t^{\mathbf{I}}) dI_t + \partial_x f(t, \tilde{X}_t^{\mathbf{I}}) f(t, \tilde{X}_t^{\mathbf{I}}) d\mathbb{I}_t + g(t, \tilde{X}_t^{\mathbf{I}}) \mathbf{v}_t^{\mathbf{I}} dB_t \\ &= \left(f(t, \tilde{X}_t^{\mathbf{I}}) + \partial_x f(t, \tilde{X}_t^{\mathbf{I}}) f(t, \tilde{X}_t^{\mathbf{I}}) \langle \mathbf{p}, \widehat{\mathbb{W}}_t^{\infty} \rangle \right) d\langle \mathbf{p}, \widehat{\mathbb{W}}_t^{\infty} \rangle + g(t, \tilde{X}_t^{\mathbf{I}}) \langle \boldsymbol{\ell}, \widehat{\mathbb{W}}_t^{\infty} \rangle dB_t \\ &= \left(f(t, \tilde{X}_t^{\mathbf{I}}) + \partial_x f(t, \tilde{X}_t^{\mathbf{I}}) f(t, \tilde{X}_t^{\mathbf{I}}) \langle \mathbf{p}, \widehat{\mathbb{W}}_t^{\infty} \rangle \right) \langle \boldsymbol{\ell}, \widehat{\mathbb{W}}_t^{\infty} \rangle dW_t + g(t, \tilde{X}_t^{\mathbf{I}}) \langle \boldsymbol{\ell}, \widehat{\mathbb{W}}_t^{\infty} \rangle dB_t \\ &= \langle f(t, \tilde{X}_t^{\mathbf{I}}) \boldsymbol{\ell} + \partial_x f(t, \tilde{X}_t^{\mathbf{I}}) f(t, \tilde{X}_t^{\mathbf{I}}) \mathbf{p} \sqcup \boldsymbol{\ell}, \widehat{\mathbb{W}}_t^{\infty} \rangle dW_t + \langle g(t, \tilde{X}_t^{\mathbf{I}}) \boldsymbol{\ell}, \widehat{\mathbb{W}}_t^{\infty} \rangle dB_t \\ &= \langle \tilde{\mathbf{q}}_t^f, \widehat{\mathbb{W}}_t^{\infty} \rangle dW_t + \langle \tilde{\mathbf{q}}_t^g, \widehat{\mathbb{W}}_t^{\infty} \rangle dB_t, \quad t \in [0, T], \end{aligned}$$

where

$$\tilde{\mathbf{q}}_t^f := f(t, \tilde{X}_t^{\mathbf{I}}) \boldsymbol{\ell} + \partial_x f(t, \tilde{X}_t^{\mathbf{I}}) f(t, \tilde{X}_t^{\mathbf{I}}) \mathbf{p} \sqcup \boldsymbol{\ell}, \quad \tilde{\mathbf{q}}_t^g := g(t, \tilde{X}_t^{\mathbf{I}}) \boldsymbol{\ell}.$$

□

A.2 Proof of Theorem 2.1

Proof. This proof is given by an application of the factorial decay property (see, e.g., Kidger et al. (2019), Proposition A.5) and the number of components of path signatures (see, e.g., Kidger et al. (2019), Remark A.11).

$$\begin{aligned} \left| \langle \boldsymbol{\ell}_t, \widehat{\mathbb{W}}_t^{\infty} \rangle - \langle \pi_{\leq N}(\boldsymbol{\ell}_t), \widehat{\mathbb{W}}_t^N \rangle \right| &= \left| \sum_{n=N+1}^{\infty} \langle \boldsymbol{\ell}_t^{(n)}, \widehat{\mathbb{W}}_t^{(n)} \rangle \right| \leq \sum_{n=N+1}^{\infty} 2^n \left\| \boldsymbol{\ell}_t^{(n)} \right\|_{\infty} \left\| \widehat{\mathbb{W}}_t^{(n)} \right\|_{\infty} \\ &\leq \sup_{t \in [0, T]} \left\| \boldsymbol{\ell}_t \right\|_{\infty} \sum_{n=N+1}^{\infty} 2^n \frac{C((\widehat{W}_t)_{t \in [0, T]})^n}{n!} \\ &= \sup_{t \in [0, T]} \left\| \boldsymbol{\ell}_t \right\|_{\infty} \frac{(2C((\widehat{W}_t)_{t \in [0, T]}))^{N+1}}{(N+1)!} \left(1 + \frac{|2C((\widehat{W}_t)_{t \in [0, T]})|}{N+2} + \frac{|2C((\widehat{W}_t)_{t \in [0, T]})|^2}{(N+2)(N+3)} + \dots \right) \\ &\leq \sup_{t \in [0, T]} \left\| \boldsymbol{\ell}_t \right\|_{\infty} \frac{(2C((\widehat{W}_t)_{t \in [0, T]}))^{N+1}}{(N+1)!} \sum_{n=0}^{\infty} \left(\frac{|2C((\widehat{W}_t)_{t \in [0, T]})|}{(N+2)} \right)^n \end{aligned}$$

$$\begin{aligned}
&= \sup_{t \in [0, T]} \|\ell_t\|_\infty \frac{(2C((\widehat{W}_t)_{t \in [0, T]}))^{N+1}}{(N+1)!} \frac{N+2}{N+2-2C((\widehat{W}_t)_{t \in [0, T]})} \\
&= O\left(\frac{(2C((\widehat{W}_t)_{t \in [0, T]}))^{N+1}}{(N+1)!}\right),
\end{aligned}$$

where $\|\cdot\|_\infty$ denotes the infinity norm. It is also easy to verify that $N \rightarrow \infty$ leads to the right-hand side of the inequality above converging to 0. \square

A.3 Proof of Proposition 2.2

Proof. This proof is given by an application of Theorem 2.1. A direct application of the extreme value theorem to g yields

$$\left| \langle \mathbf{q}_t^g, \widehat{\mathbb{W}}_t^\infty \rangle - \langle \pi_{\leq N}(\mathbf{q}_t^g), \widehat{\mathbb{W}}_t^N \rangle \right| \leq \sup_{(s, y) \in \Omega} g(s, y) G_t^{\ell, N}.$$

Similarly, we have

$$\begin{aligned}
&\left| \langle \mathbf{q}_t^f, \widehat{\mathbb{W}}_t^\infty \rangle - \langle \pi_{\leq N}(\mathbf{q}_t^f), \widehat{\mathbb{W}}_t^N \rangle \right| \leq \sup_{(s, y) \in \Omega} f(s, y) G_t^{\ell, N} + \sup_{(s, y) \in \Omega} f(s, y) \sup_{(s, y) \in \Omega} \partial_y f(s, y) \\
&\left| \left\langle \int_0^t \langle \ell_s, \widehat{\mathbb{W}}_s^\infty \rangle dW_s \ell_t, \widehat{\mathbb{W}}_t^\infty \right\rangle - \left\langle \int_0^t \langle \pi_{\leq N}(\ell_s), \widehat{\mathbb{W}}_s^N \rangle dW_s \pi_{\leq N}(\ell_t), \widehat{\mathbb{W}}_t^N \right\rangle \right|.
\end{aligned}$$

Consider

$$\begin{aligned}
&\left| \left\langle \int_0^t \langle \ell_s, \widehat{\mathbb{W}}_s^\infty \rangle dW_s \ell_t, \widehat{\mathbb{W}}_t^\infty \right\rangle - \left\langle \int_0^t \langle \pi_{\leq N}(\ell_s), \widehat{\mathbb{W}}_s^N \rangle dW_s \pi_{\leq N}(\ell_t), \widehat{\mathbb{W}}_t^N \right\rangle \right| \\
&\leq \left| \left\langle \int_0^t \langle \ell_s, \widehat{\mathbb{W}}_s^\infty \rangle dW_s \ell_t, \widehat{\mathbb{W}}_t^\infty \right\rangle - \left\langle \int_0^t \langle \ell_s, \widehat{\mathbb{W}}_s^\infty \rangle dW_s \pi_{\leq N}(\ell_t), \widehat{\mathbb{W}}_t^N \right\rangle \right| \\
&+ \left| \left\langle \int_0^t \langle \ell_s, \widehat{\mathbb{W}}_s^\infty \rangle dW_s \pi_{\leq N}(\ell_t), \widehat{\mathbb{W}}_t^N \right\rangle - \left\langle \int_0^t \langle \pi_{\leq N}(\ell_s), \widehat{\mathbb{W}}_s^N \rangle dW_s \pi_{\leq N}(\ell_t), \widehat{\mathbb{W}}_t^N \right\rangle \right|.
\end{aligned}$$

For the first part, we have

$$\left| \left\langle \int_0^t \langle \ell_s, \widehat{\mathbb{W}}_s^\infty \rangle dW_s \ell_t, \widehat{\mathbb{W}}_t^\infty \right\rangle - \left\langle \int_0^t \langle \ell_s, \widehat{\mathbb{W}}_s^\infty \rangle dW_s \pi_{\leq N}(\ell_t), \widehat{\mathbb{W}}_t^N \right\rangle \right| \leq \int_0^t |\langle \ell_s, \widehat{\mathbb{W}}_s^\infty \rangle| dW_s G_t^{\ell, N}.$$

For the second part, we have

$$\begin{aligned}
&\left| \left\langle \int_0^t \langle \ell_s, \widehat{\mathbb{W}}_s^\infty \rangle dW_s \pi_{\leq N}(\ell_t), \widehat{\mathbb{W}}_t^N \right\rangle - \left\langle \int_0^t \langle \pi_{\leq N}(\ell_s), \widehat{\mathbb{W}}_s^N \rangle dW_s \pi_{\leq N}(\ell_t), \widehat{\mathbb{W}}_t^N \right\rangle \right| \\
&= \left| \left\langle \int_0^t (\langle \ell_s, \widehat{\mathbb{W}}_s^\infty \rangle - \langle \pi_{\leq N}(\ell_s), \widehat{\mathbb{W}}_s^N \rangle) dW_s \pi_{\leq N}(\ell_t), \widehat{\mathbb{W}}_t^N \right\rangle \right| \leq \int_0^t G_s^{\ell, N} dW_s |\langle \pi_{\leq N}(\ell_t), \widehat{\mathbb{W}}_t^N \rangle|.
\end{aligned}$$

With above, we finally have

$$\begin{aligned}
&\left| \langle \mathbf{q}_t^f, \widehat{\mathbb{W}}_t^\infty \rangle - \langle \pi_{\leq N}(\mathbf{q}_t^f), \widehat{\mathbb{W}}_t^N \rangle \right| \leq \sup_{(s, y) \in \Omega} f(s, y) G_t^{\ell, N} + \sup_{(s, y) \in \Omega} f(s, y) \sup_{(s, y) \in \Omega} \partial_y f(s, y) \\
&\left(\int_0^t |\langle \ell_s, \widehat{\mathbb{W}}_s^\infty \rangle| dW_s G_t^{\ell, N} + \int_0^t G_s^{\ell, N} dW_s |\langle \pi_{\leq N}(\ell_t), \widehat{\mathbb{W}}_t^N \rangle| \right).
\end{aligned}$$

\square

A.4 Proof of Theorem 2.2

Proof. This proof is given by an application of Proposition 2.2.

$$\begin{aligned}
|u(0, x) - u^N(0, x)| &= |\mathbb{E} [\Phi(X_T^{\mathbf{I}})] - \mathbb{E} [\Phi(X_T^{\mathbf{I}, N})]| \leq \mathbb{E} [|\Phi(X_T^{\mathbf{I}}) - \Phi(X_T^{\mathbf{I}, N})|] \leq \mathcal{L} \cdot \mathbb{E} [|X_T^{\mathbf{I}} - X_T^{\mathbf{I}, N}|] \\
&\leq \mathcal{L} \cdot \mathbb{E} \left[\left| \int_0^T C_1((\widehat{W}_t)_{t \in [0, T]}, N, f, \ell) dW_t + \int_0^T C_2((\widehat{W}_t)_{t \in [0, T]}, N, g, \ell) dB_t \right| \right] \\
&\leq \mathcal{L} \cdot \mathbb{E} \left[\left| \int_0^T C_1((\widehat{W}_t)_{t \in [0, T]}, N, f, \ell) dW_t \right| \right] + \mathcal{L} \cdot \mathbb{E} \left[\left| \int_0^T C_2((\widehat{W}_t)_{t \in [0, T]}, N, g, \ell) dB_t \right| \right]
\end{aligned} \tag{33}$$

where

$$\begin{aligned}
C_1((\widehat{W}_t)_{t \in [0, T]}, N, f, \ell) &:= \sup_{(s, y) \in \Omega} f(s, y) G_t^{\ell, N} + \sup_{(s, y) \in \Omega} f(s, y) \sup_{(s, y) \in \Omega} \partial_y f(s, y) \\
&\quad \left(\int_0^t \langle \ell_s, \widehat{\mathbb{W}}_s^\infty \rangle dW_s G_t^{\ell, N} + \int_0^t G_s^{\ell, N} dW_s \langle \pi_{\leq N}(\ell_t), \widehat{\mathbb{W}}_t^{\leq N} \rangle \right),
\end{aligned}$$

and

$$C_2((\widehat{W}_t)_{t \in [0, T]}, N, g, \ell) := \sup_{(s, y) \in \Omega} g(s, y) G_t^{\ell, N}.$$

For simplicity, we omit the arguments of C_1 and C_2 without ambiguity in the following context. We further deal with C_1 as follows

$$\begin{aligned}
C_1 &= \sup_{(s, y) \in \Omega} f(s, y) G_t^{\ell, N} + \sup_{(s, y) \in \Omega} f(s, y) \sup_{(s, y) \in \Omega} \partial_y f(s, y) \\
&\quad \left(\int_0^t \left| \sum_{n=0}^{\infty} \langle \ell_s^{(n)}, \widehat{\mathbb{W}}_s^{(n)} \rangle \right| dW_s G_t^{\ell, N} + \int_0^t G_s^{\ell, N} dW_s \left| \sum_{n=0}^N \langle \ell_t^{(n)}, \widehat{\mathbb{W}}_t^{(n)} \rangle \right| \right) \\
&\leq \sup_{(s, y) \in \Omega} f(s, y) G_t^{\ell, N} + \sup_{(s, y) \in \Omega} f(s, y) \sup_{(s, y) \in \Omega} \partial_y f(s, y) \\
&\quad \left(\int_0^t \sum_{n=0}^{\infty} \langle \ell_s^{(n)}, \widehat{\mathbb{W}}_s^{(n)} \rangle dW_s G_t^{\ell, N} + \int_0^t G_s^{\ell, N} dW_s \left(\sum_{n=0}^{\infty} \langle \ell_t^{(n)}, \widehat{\mathbb{W}}_t^{(n)} \rangle \right) \right) \\
&\leq \sup_{(s, y) \in \Omega} f(s, y) \sup_{t \in [0, T]} G_t^{\ell, N} \left(1 + 2 \sup_{(s, y) \in \Omega} \partial_y f(s, y) \sup_{t \in [0, T]} \|\ell_t\|_{\infty} e^{2|C((\widehat{W}_t)_{t \in [0, T]})|} \int_0^t dW_s \right).
\end{aligned} \tag{34}$$

Define constant $C \geq 2C((\widehat{W}_t)_{t \in [0, T]})$ for all paths, then for the first term of (33), we have

$$\begin{aligned}
\mathbb{E} \left[\left| \int_0^T C_1 dW_t \right| \right] &\leq \left(\mathbb{E} \left[\left(\int_0^T C_1 dW_t \right)^2 \right] \right)^{\frac{1}{2}} = \left(\mathbb{E} \left[\int_0^T C_1^2 dt \right] \right)^{\frac{1}{2}} = \left[\int_0^T \mathbb{E} (C_1^2) dt \right]^{\frac{1}{2}} \\
&\leq \sqrt{T + T^2} \cdot O \left(\frac{C^{N+1}}{(N+1)!} \right),
\end{aligned}$$

where the first equality uses the Itô isometry and the last inequality is obtained by applying (34). Similarly, for the second term, we have

$$\mathbb{E} \left[\left| \int_0^T C_2 dB_t \right| \right] \leq \left(\mathbb{E} \left[\left(\int_0^T C_2 dB_t \right)^2 \right] \right)^{\frac{1}{2}} = \left(\mathbb{E} \left[\int_0^T C_2^2 dt \right] \right)^{\frac{1}{2}} \leq \sqrt{T} \cdot O \left(\frac{C^{N+1}}{(N+1)!} \right).$$

With the above analysis, we have

$$\left| u(0, x) - u^N(0, x) \right| \leq \mathcal{L} \cdot \left(\sqrt{T^2 + T} + \sqrt{T} \right) \cdot O \left(\frac{C^{N+1}}{(N+1)!} \right).$$

□

A.5 Proof of Theorem 2.3

Proof. We first decompose the error as follows:

$$\mathbb{E} \left| v_t - \mathcal{N}_t^v(\widehat{\mathbb{W}}_t^N; \phi_v) \right| \leq \mathbb{E} \left| v_t - \mathcal{L}(\widehat{\mathbb{W}}_t^\infty) \right| + \mathbb{E} \left| \mathcal{L}(\widehat{\mathbb{W}}_t^\infty) - \mathcal{L}(\widehat{\mathbb{W}}_t^N) \right| + \mathbb{E} \left| \mathcal{L}(\widehat{\mathbb{W}}_t^N) - \mathcal{N}_t^v(\widehat{\mathbb{W}}_t^N; \phi_v) \right|, \quad (35)$$

where \mathcal{L} denotes a linear functional. According to the universal nonlinearity proposition (see, e.g., [Kidger et al. \(2019\)](#), Proposition A.6), for (\mathcal{F}_t^W) -progressive and continuous stochastic process v and any $\epsilon_t^{\mathcal{N}, v, 1} > 0$, there exists a linear functional \mathcal{L} depending on a compact set, such that

$$\mathbb{E} \left| v_t - \mathcal{L}(\widehat{\mathbb{W}}_t^\infty) \right| \leq \epsilon_t^{\mathcal{N}, v, 1}.$$

The second term of (35) can be estimated by Theorem 2.1 as follows

$$\mathbb{E} \left| \mathcal{L}(\widehat{\mathbb{W}}_t^\infty) - \mathcal{L}(\widehat{\mathbb{W}}_t^N) \right| \leq O \left(\frac{\left(2C((\widehat{W}_t)_{t \in [0, T]}) \right)^{N+1}}{(N+1)!} \right) := \epsilon_t^{\mathcal{N}, v, N}.$$

Next, applying the universality property (see, e.g., [Funahashi and Nakamura \(1993\)](#)), for the linear functional and any $\epsilon_t^{\mathcal{N}, v, 2} > 0$, there exists a neural network $\mathcal{N}_t^v(\widehat{\mathbb{W}}_t^N; \phi_v)$, such that

$$\mathbb{E} \left| \mathcal{L}(\widehat{\mathbb{W}}_t^N) - \mathcal{N}_t^v(\widehat{\mathbb{W}}_t^N; \phi_v) \right| \leq \epsilon_t^{\mathcal{N}, v, 2}.$$

Combining the above estimates, for a fixed neural network at time t , we conclude that

$$\mathcal{E}_t^{\mathcal{N}, v} \leq \epsilon_t^{\mathcal{N}, v, 1} + \epsilon_t^{\mathcal{N}, v, 2} + \epsilon_t^{\mathcal{N}, v, N} := \epsilon_t^{\mathcal{N}, v} + \epsilon_t^{\mathcal{N}, v, N}.$$

□